Mathematics

https://www.aimspress.com/journal/Math

AIMS Mathematics, 11(9): 29256–29284.
DOI: 10.3934/math.20261163
Received: 29 April 2026
Revised: 08 July 2026
Accepted: 15 July 2026
Published: 11 September 2026

Research article

Bicubic B-spline Galerkin method for solving the two-dimensional nonlinear Schrödinger equation

Emad Omar Altahat[1], **Nur Nadiah Abd Hamid**[2], **Adila Aida Azahar**[1,*] **and Yazariah Mohd Yatim**[1]

[1] School of Mathematical Sciences, Universiti Sains Malaysia, 11800 USM, Penang, Malaysia
[2] Nur Nadiah Academic Services, Butterworth 13800, Penang, Malaysia

* **Correspondence:** Email: adilaazahar@usm.my.

Abstract: The nonlinear Schrödinger (NLS) equation appears in many physical contexts, such as nonlinear optics, quantum mechanics, and wave propagation. This paper introduces a Galerkin finite-element method based on bicubic B-spline basis functions for solving the two-dimensional time-dependent NLS equation. The spatial discretization was carried out using bicubic B-splines within a Galerkin framework, while time integration was performed using the Crank-Nicolson scheme, resulting in a fully discrete formulation. Bicubic B-spline basis functions provide higher smoothness across element interfaces and offer better approximation properties compared with standard polynomial finite-element spaces. Linear stability was investigated under periodic boundary conditions using the von Neumann method. A plane wave test problem was used to assess the accuracy, stability, and convergence behavior of the proposed method. To supplement the plane-wave test, a spatially varying amplitude benchmark was included to examine the nonlinear two-dimensional dynamics and the long-time evolution of the discrete mass and Hamiltonian invariants, denoted by I_1 and I_2, respectively. The numerical results indicated stable two-dimensional performance, with convergence rates close to second order in both space and time, while the nonconstant-amplitude benchmark illustrated the distinct long-time behavior of the discrete I_1 and I_2 invariants.

Keywords: two-dimensional NLS equation; bicubic B-spline Galerkin method; Crank-Nicolson time discretization; numerical stability; convergence behavior
Mathematics Subject Classification: 65N30, 65M60, 35Q55

1. Introduction

The nonlinear Schrödinger (NLS) equation is widely used to model a variety of physical processes arising in nonlinear optics, quantum mechanics, plasma physics, and wave propagation in dispersive media. The interplay between nonlinearity and dispersion makes the accurate numerical simulation of the NLS equation particularly challenging, especially in two and higher spatial dimensions. As a consequence, the development of numerical methods that are both stable and reliable has remained an active area of research over the past several decades. Although the present study focuses on the numerical approximation of the two-dimensional NLS equation, recent analytical studies have also investigated generalized NLS models using soliton-based approaches. For example, Yu and Yu [1] investigated non-autonomous soliton propagation, wave propagation, and collision dynamics for a (2+1)-dimensional, variable-coefficient, higher-order NLS equation, while Zhou and Yu [2] examined space-time-shifted solitons and solution interactions for a generalized, nonlocal, nonlinear Schrödinger equation.

A broad range of numerical techniques has been proposed for the approximation of the NLS equation. Finite difference and spectral-type methods have been extensively investigated and have demonstrated good performance in many applications [3, 4]. However, such methods may face difficulties in higher-dimensional settings or when highly smooth and flexible approximation spaces are required. The finite element method (FEM) offers a natural alternative, as it utilizes complex spatial discretization and is well-suited for multidimensional problems.

The Galerkin FEM is a well-established framework for numerically solving parabolic and Schrödinger-type equations, due to its stability properties [5–7]. For NLS equations, Galerkin-based formulations have demonstrated reliable accuracy and robustness in both one- and two-dimensional (2D) settings [8–10]. The Crank-Nicolson (CN) formulation is frequently combined with Galerkin spatial discretization due to its stability features and second-order temporal accuracy [9, 11, 12].

On the other hand, spline-based finite element and collocation methods have gained growing attention in solving nonlinear partial differential equations [13–15]. B-spline basis functions introduce higher smoothness and better approximation properties compared with standard polynomial finite-element spaces, which can lead to better accuracy for a fixed number of degrees of freedom. Therefore, a variety of B-spline-based schemes have been applied to Schrödinger-type equations, including cubic, quartic, and higher-order spline approximations [16–18]. Bicubic B-spline finite-element formulations have shown good performance in solving Laplace, Burgers-type, and convection–diffusion equations [19–21], highlighting their ability to generate smooth and accurate spatial approximations in multidimensional settings [22].

Despite these developments, the numerical analysis of 2D NLS equations based on spline-based Galerkin FEMs is still limited. A significant amount of available literature focuses either on one-dimensional (1D) problems or on alternative discretization strategies, while systematic studies that combine smooth spline-based spatial approximations with implicit time integration in two spatial dimensions are infrequent. Recent studies have highlighted the importance of developing stable and accurate numerical schemes for NLS-type equations, including conventional formulations, Galerkin-based approaches, and spline-based techniques [23–25], as well as low-regularity integrators for random-potential models [26], exponential-type dispersion-map integrators for soliton-management problems [27], and relaxation schemes with local discontinuous Galerkin methods for shock-type initial data [28]. These studies revealed the need for numerical methods capable of delivering good performance in multidimensional settings.

Addressing the need, this paper introduces a Galerkin FEM based on bicubic B-spline basis functions for solving the 2D, time-dependent NLS equation, whereby the time discretization is carried out using the CN scheme, leading to a fully discrete formulation that joins implicit time integration with the smoothness features of spline-based spatial approximations. The proposed method is then evaluated using stability analysis under periodic boundary conditions.

The primary contributions of this study are summarized as follows:

- A bicubic B-spline Galerkin finite-element formulation is developed for the 2D NLS equation.
- The Galerkin spatial discretization is combined with CN time integration to get a stable fully discrete scheme.
- The stability and convergence behavior of the proposed method are tested.
- Numerical experiments are presented to show the accuracy and robustness of the approach in two spatial dimensions.

The paper is organized as follows. Section 2 presents the mathematical model of the 2D NLS equation and the bicubic B-spline Galerkin formulation, including the associated notation and the CN time discretization. Section 3 is devoted to the stability analysis of the proposed scheme. Numerical results illustrating the accuracy, stability, and convergence behavior are presented in Section 4. Finally, concluding remarks are given in Section 5.

2. Bicubic B-spline Galerkin method

2.1. Formulation of the method

Let $\Omega = [a,b] \times [c,d] \subset \mathbb{R}^2$ denote a rectangular spatial domain, and let $t \in [0,T]$, where T denotes the final time. The time-dependent 2D NLS equation is given by

$$\mathrm{i}\frac{\partial u}{\partial t} + \Delta u + q|u|^2 u = 0, \qquad (x,y) \in \Omega,\ t > 0, \tag{2.1}$$

with the initial condition

$$u(x,y,0) = f(x,y), \qquad (x,y) \in \Omega, \tag{2.2}$$

and periodic boundary conditions

$$\begin{aligned} u(a,y,t) &= u(b,y,t), & u(x,c,t) &= u(x,d,t), \\ u_x(a,y,t) &= u_x(b,y,t), & u_y(x,c,t) &= u_y(x,d,t), \\ u_{xx}(a,y,t) &= u_{xx}(b,y,t), & u_{yy}(x,c,t) &= u_{yy}(x,d,t), \qquad & (x,y) \in \Omega,\ 0 \le t \le T. \end{aligned} \tag{2.3}$$

For numerical implementation, the complex-valued solution is decomposed as

$$u(x,y,t) = r(x,y,t) + \mathrm{i}s(x,y,t), \tag{2.4}$$

which leads to the coupled system

$$\begin{aligned} s_t - \Delta r - q(r^2 + s^2)r &= 0, \\ r_t + \Delta s + q(r^2 + s^2)s &= 0. \end{aligned} \tag{2.5}$$

Consider the 1D cubic B-spline basis functions $B_i(x)$ and $B_j(y)$. A bicubic tensor product basis is then formed as [22]

$$B_{i,j}(x,y) = B_i(x)B_j(y), \tag{2.6}$$

which yields a C^2-continuous basis over the rectangular domain $\Omega = [a, b] \times [c, d]$.

The computational domain Ω is partitioned into $N \times M$ uniform rectangular elements with mesh sizes

$$h_x = \frac{b-a}{N}, \qquad h_y = \frac{d-c}{M}.$$

Let $\{x_l\}_{l=0}^{N}$ and $\{y_k\}_{k=0}^{M}$ represent the grid points in the x- and y-directions, respectively. Therefore, the bicubic B-spline basis is defined on these grids as follows:

$$B_{l,k}(x,y) = \frac{1}{h_x^3 h_y^3}\begin{cases} p_{c1}q_{c1}, & [x_{l-2}, x_{l-1}] \times [y_{k-2}, y_{k-1}], \\ p_{c2}q_{c1}, & [x_{l-2}, x_{l-1}] \times [y_{k-1}, y_{k}], \\ p_{c3}q_{c1}, & [x_{l-2}, x_{l-1}] \times [y_{k}, y_{k+1}], \\ p_{c4}q_{c1}, & [x_{l-2}, x_{l-1}] \times [y_{k+1}, y_{k+2}], \\ p_{c1}q_{c2}, & [x_{l-1}, x_{l}] \times [y_{k-2}, y_{k-1}], \\ p_{c2}q_{c2}, & [x_{l-1}, x_{l}] \times [y_{k-1}, y_{k}], \\ p_{c3}q_{c2}, & [x_{l-1}, x_{l}] \times [y_{k}, y_{k+1}], \\ p_{c4}q_{c2}, & [x_{l-1}, x_{l}] \times [y_{k+1}, y_{k+2}], \\ p_{c1}q_{c3}, & [x_{l}, x_{l+1}] \times [y_{k-2}, y_{k-1}], \\ p_{c2}q_{c3}, & [x_{l}, x_{l+1}] \times [y_{k-1}, y_{k}], \\ p_{c3}q_{c3}, & [x_{l}, x_{l+1}] \times [y_{k}, y_{k+1}], \\ p_{c4}q_{c3}, & [x_{l}, x_{l+1}] \times [y_{k+1}, y_{k+2}], \\ p_{c1}q_{c4}, & [x_{l+1}, x_{l+2}] \times [y_{k-2}, y_{k-1}], \\ p_{c2}q_{c4}, & [x_{l+1}, x_{l+2}] \times [y_{k-1}, y_{k}], \\ p_{c3}q_{c4}, & [x_{l+1}, x_{l+2}] \times [y_{k}, y_{k+1}], \\ p_{c4}q_{c4}, & [x_{l+1}, x_{l+2}] \times [y_{k+1}, y_{k+2}], \\ 0, & \text{otherwise}, \end{cases} \tag{2.7}$$

where

$$\begin{aligned} p_{c1} &= (x - x_{l-2})^3, \\ p_{c2} &= h_x^3 + 3h_x^2(x - x_{l-1}) + 3h_x(x - x_{l-1})^2 - 3(x - x_{l-1})^3, \\ p_{c3} &= h_x^3 + 3h_x^2(x_{l+1} - x) + 3h_x(x_{l+1} - x)^2 - 3(x_{l+1} - x)^3, \\ p_{c4} &= (x_{l+2} - x)^3, \\ q_{c1} &= (y - y_{k-2})^3, \\ q_{c2} &= h_y^3 + 3h_y^2(y - y_{k-1}) + 3h_y(y - y_{k-1})^2 - 3(y - y_{k-1})^3, \\ q_{c3} &= h_y^3 + 3h_y^2(y_{k+1} - y) + 3h_y(y_{k+1} - y)^2 - 3(y_{k+1} - y)^3, \\ q_{c4} &= (y_{k+2} - y)^3. \end{aligned}$$

The approximate solution for the NLS equation is generated from the bicubic B-spline basis as

$$u_{N,M}(x,y,t) = r_{N,M}(x,y,t) + \mathrm{i}\, s_{N,M}(x,y,t) = \sum_{i=-1}^{N+1}\sum_{j=-1}^{M+1} \delta_{i,j}(t)\, B_{i,j}(x,y), \tag{2.8}$$

where $\delta_{i,j}(t) = \rho_{i,j}(t) + \mathrm{i}\,\psi_{i,j}(t)$ are time-dependent complex coefficients. Accordingly, the approximate solutions can be separated as

$$
\begin{aligned}
r_{N,M}(x,y,t) &= \sum_{i=-1}^{N+1}\sum_{j=-1}^{M+1} \rho_{i,j}(t)\, B_{i,j}(x,y),\\
s_{N,M}(x,y,t) &= \sum_{i=-1}^{N+1}\sum_{j=-1}^{M+1} \psi_{i,j}(t)\, B_{i,j}(x,y).
\end{aligned}
\tag{2.9}
$$

The time-dependent coefficients $\rho_{i,j}(t)$ and $\psi_{i,j}(t)$ are determined through the Galerkin weighted-residual approach. Periodic boundary conditions are enforced at the discrete level by identifying the degrees of freedom associated with basis functions on opposite boundaries; equivalently, the coefficient sets corresponding to $x = a$ and $x = b$ (and similarly for $y = c$ and $y = d$) are constrained to be equal. In matrix form, this identification may be expressed using a restriction operator R such that $\mathbf{u} = R\tilde{\mathbf{u}}$, where $\tilde{\mathbf{u}}$ denotes the vector of all degrees of freedom before applying periodic constraints, and $\mathbf{u}$ is the reduced vector after enforcing periodicity.

Due to the compact support in cubic B-splines, each bicubic tensor product basis function $B_{i,j}(x,y)$ has support over 4×4 neighboring elements. Hence, on a given element $[x_l, x_{l+1}]\times[y_k, y_{k+1}]$, only 16 basis functions are nonzero. Introducing the local coordinates $\mu = x - x_l \in [0, h_x]$ and $\eta = y - y_k \in [0, h_y]$, the nonzero bicubic basis functions on the element can be written explicitly as follows:

$$
\begin{aligned}
B_{l-1,k-1} &= \frac{1}{h_x^3 h_y^3}(h_x-\mu)^3(h_y-\eta)^3,\\
B_{l-1,k} &= \frac{1}{h_x^3 h_y^3}(h_x-\mu)^3\left(4h_y^3 - 3h_y^2\eta + 3h_y(h_y-\eta) - 3(h_y-\eta)^3\right),\\
B_{l-1,k+1} &= \frac{1}{h_x^3 h_y^3}(h_x-\mu)^3\left(h_y^3 + 3h_y^2\eta + 3h_y\eta^2 - 3\eta^3\right),\\
B_{l-1,k+2} &= \frac{1}{h_x^3 h_y^3}(h_x-\mu)^3\eta^3,\\
B_{l,k-1} &= \frac{1}{h_x^3 h_y^3}\left(4h_x^3 - 3h_x^2\mu + 3h_x(h_x-\mu) - 3(h_x-\mu)^3\right)(h_y-\eta)^3,\\
B_{l,k} &= \frac{1}{h_x^3 h_y^3}\left(4h_x^3 - 3h_x^2\mu + 3h_x(h_x-\mu) - 3(h_x-\mu)^3\right)\\
&\quad\times\left(4h_y^3 - 3h_y^2\eta + 3h_y(h_y-\eta) - 3(h_y-\eta)^3\right),\\
B_{l,k+1} &= \frac{1}{h_x^3 h_y^3}\left(4h_x^3 - 3h_x^2\mu + 3h_x(h_x-\mu) - 3(h_x-\mu)^3\right)\\
&\quad\times\left(h_y^3 + 3h_y^2\eta + 3h_y\eta^2 - 3\eta^3\right),\\
B_{l,k+2} &= \frac{1}{h_x^3 h_y^3}\left(4h_x^3 - 3h_x^2\mu + 3h_x(h_x-\mu) - 3(h_x-\mu)^3\right)\eta^3,\\
B_{l+1,k-1} &= \frac{1}{h_x^3 h_y^3}\left(h_x^3 + 3h_x^2\mu + 3h_x\mu^2 - 3\mu^3\right)(h_y-\eta)^3,\\
B_{l+1,k} &= \frac{1}{h_x^3 h_y^3}\left(h_x^3 + 3h_x^2\mu + 3h_x\mu^2 - 3\mu^3\right)
\end{aligned}
$$

$$
\begin{aligned}
&\times\left(4h_y^3 - 3h_y^2\eta + 3h_y(h_y-\eta) - 3(h_y-\eta)^3\right),\\
B_{l+1,k+1} &= \frac{1}{h_x^3h_y^3}\left(h_x^3 + 3h_x^2\mu + 3h_x\mu^2 - 3\mu^3\right)\\
&\quad\times\left(h_y^3 + 3h_y^2\eta + 3h_y\eta^2 - 3\eta^3\right),\\
B_{l+1,k+2} &= \frac{1}{h_x^3h_y^3}\left(h_x^3 + 3h_x^2\mu + 3h_x\mu^2 - 3\mu^3\right)\eta^3,\\
B_{l+2,k-1} &= \frac{1}{h_x^3h_y^3}\mu^3(h_y-\eta)^3,\\
B_{l+2,k} &= \frac{1}{h_x^3h_y^3}\mu^3\left(4h_y^3 - 3h_y^2\eta + 3h_y(h_y-\eta) - 3(h_y-\eta)^3\right),\\
B_{l+2,k+1} &= \frac{1}{h_x^3h_y^3}\mu^3\left(h_y^3 + 3h_y^2\eta + 3h_y\eta^2 - 3\eta^3\right),\\
B_{l+2,k+2} &= \frac{1}{h_x^3h_y^3}(\mu\eta)^3.
\end{aligned}
\tag{2.10}
$$

On the element $[x_l, x_{l+1}] \times [y_k, y_{k+1}]$, all remaining bicubic B-spline basis functions are zero. Consequently, the approximation of the solution restricted to this element can be expressed, using the local basis functions defined in (2.10), as

$$
\begin{aligned}
r_{N,M}(x,y,t) &= \sum_{i=l-1}^{l+2}\sum_{j=k-1}^{k+2}\rho_{i,j}(t)\,B_{i,j}(x,y),\\
s_{N,M}(x,y,t) &= \sum_{i=l-1}^{l+2}\sum_{j=k-1}^{k+2}\psi_{i,j}(t)\,B_{i,j}(x,y).
\end{aligned}
\tag{2.11}
$$

Using the bicubic B-spline basis functions (2.7) together with the trial approximation (2.9), the nodal values of the approximate solution together with its first- and second-order partial derivatives at the grid point (x_l, y_k), can be written in terms of the time-dependent coefficients $\rho_{i,j}(t)$ and $\psi_{i,j}(t)$ as follows:

$$
\begin{aligned}
r_{l,k} &= \rho_{l-1,k-1} + 4\rho_{l-1,k} + \rho_{l-1,k+1} + 4\rho_{l,k-1} + 16\rho_{l,k} + 4\rho_{l,k+1}\\
&\quad + \rho_{l+1,k-1} + 4\rho_{l+1,k} + \rho_{l+1,k+1},\\
s_{l,k} &= \psi_{l-1,k-1} + 4\psi_{l-1,k} + \psi_{l-1,k+1} + 4\psi_{l,k-1} + 4\psi_{l,k+1} + 16\psi_{l,k}\\
&\quad + \psi_{l+1,k-1} + 4\psi_{l+1,k} + \psi_{l+1,k+1},\\
h_x\,\partial_x r_{l,k} &= 3(\rho_{l-1,k-1} + \rho_{l-1,k+1} - \rho_{l+1,k-1} - \rho_{l+1,k+1}) + 12(\rho_{l-1,k} - \rho_{l+1,k}),\\
h_x\,\partial_x s_{l,k} &= 3(\psi_{l-1,k-1} + \psi_{l-1,k+1} - \psi_{l+1,k-1} - \psi_{l+1,k+1}) + 12(\psi_{l-1,k} - \psi_{l+1,k}),\\
h_y\,\partial_y r_{l,k} &= 3(\rho_{l-1,k-1} + \rho_{l+1,k-1} - \rho_{l-1,k+1} - \rho_{l+1,k+1}) + 12(\rho_{l,k-1} - \rho_{l,k+1}),\\
h_y\,\partial_y s_{l,k} &= 3(\psi_{l-1,k-1} + \psi_{l+1,k-1} - \psi_{l-1,k+1} - \psi_{l+1,k+1}) + 12(\psi_{l,k-1} - \psi_{l,k+1}),\\
h_xh_y\,\partial_{xy} r_{l,k} &= 9(\rho_{l-1,k-1} + \rho_{l+1,k+1} - \rho_{l-1,k+1} - \rho_{l+1,k-1}),\\
h_xh_y\,\partial_{xy} s_{l,k} &= 9(\psi_{l-1,k-1} + \psi_{l+1,k+1} - \psi_{l-1,k+1} - \psi_{l+1,k-1}),
\end{aligned}
\tag{2.12}
$$

where ∂_x and ∂_y denote the first-order partial derivatives with respect to x and y, respectively, while ∂_{xx}, ∂_{yy}, and ∂_{xy} denote the corresponding second-order partial derivatives.

Applying the Galerkin method to the coupled system (2.5), and choosing the bicubic B-spline basis functions as weight (test) functions, the weak formulation is enforced locally over each finite element $[x_l, x_{l+1}] \times [y_k, y_{k+1}]$. Within the Galerkin framework, the weight function $W(x, y)$ is selected from the same finite-element space as the trial function. Consequently, the following element-level equations are obtained:

$$\begin{aligned} &\int_{x_l}^{x_{l+1}} \int_{y_k}^{y_{k+1}} (W\, s_t + \nabla W \cdot \nabla r - z_{l,k}\, W\, r)\, dy\, dx = 0, \\ &\int_{x_l}^{x_{l+1}} \int_{y_k}^{y_{k+1}} (W\, r_t - \nabla W \cdot \nabla s + z_{l,k}\, W\, s)\, dy\, dx = 0, \end{aligned} \tag{2.13}$$

where

$$z_{l,k} = q\left(r^2 + s^2\right). \tag{2.14}$$

Choosing the weight function as the bicubic B-spline basis function $W(x, y) = B_{n,m}(x, y)$, substituting the local approximations (2.11) into the element-level weak formulation (2.13), and transforming the equation into the local coordinates (μ, η) results in the following system of ordinary differential equations:

$$\begin{aligned} &\sum_{i=l-1}^{l+2} \sum_{j=k-1}^{k+2} \Bigg[\int_0^{h_x}\int_0^{h_y} \left(B_{n,m} B_{i,j}\, d\mu\, d\eta\right) \dot{\psi}_{i,j} + \int_0^{h_x}\int_0^{h_y} \left(\nabla B_{n,m} \cdot \nabla B_{i,j}\, d\mu\, d\eta\right) \rho_{i,j} \\ &\qquad - z_{l,k} \int_0^{h_x}\int_0^{h_y} \left(B_{n,m} B_{i,j}\, d\mu\, d\eta\right) \rho_{i,j} \Bigg] = 0, \\ &\sum_{i=l-1}^{l+2} \sum_{j=k-1}^{k+2} \Bigg[\int_0^{h_x}\int_0^{h_y} \left(B_{n,m} B_{i,j}\, d\mu\, d\eta\right) \dot{\rho}_{i,j} - \int_0^{h_x}\int_0^{h_y} \left(\nabla B_{n,m} \cdot \nabla B_{i,j}\, d\mu\, d\eta\right) \psi_{i,j} \\ &\qquad + z_{l,k} \int_0^{h_x}\int_0^{h_y} \left(B_{n,m} B_{i,j}\, d\mu\, d\eta\right) \psi_{i,j} \Bigg] = 0. \end{aligned} \tag{2.15}$$

System (2.15) can be expressed in the following compact form:

$$\begin{cases} A^e\, \dot{\boldsymbol{\psi}}^e + B^e\, \boldsymbol{\rho}^e - z_{l,k}\, D^e\, \boldsymbol{\rho}^e = \mathbf{0}, \\ A^e\, \dot{\boldsymbol{\rho}}^e - B^e\, \boldsymbol{\psi}^e + z_{l,k}\, D^e\, \boldsymbol{\psi}^e = \mathbf{0}, \end{cases} \tag{2.16}$$

where the overdot $(\dot{})$ represents differentiation with respect to t and the element coefficient vector $\boldsymbol{\rho}^e$ is defined as

$$\begin{aligned} \boldsymbol{\rho}^e = [&\rho_{l-1,k-1}, \rho_{l-1,k}, \rho_{l-1,k+1}, \rho_{l-1,k+2}, \rho_{l,k-1}, \rho_{l,k}, \rho_{l,k+1}, \rho_{l,k+2}, \\ &\rho_{l+1,k-1}, \rho_{l+1,k}, \rho_{l+1,k+1}, \rho_{l+1,k+2}, \rho_{l+2,k-1}, \rho_{l+2,k}, \rho_{l+2,k+1}, \rho_{l+2,k+2}]^T. \end{aligned}$$

Similarly, the element coefficient vector $\boldsymbol{\psi}^e$ is given by

$$\begin{aligned} \boldsymbol{\psi}^e = [&\psi_{l-1,k-1}, \psi_{l-1,k}, \psi_{l-1,k+1}, \psi_{l-1,k+2}, \psi_{l,k-1}, \psi_{l,k}, \psi_{l,k+1}, \psi_{l,k+2}, \\ &\psi_{l+1,k-1}, \psi_{l+1,k}, \psi_{l+1,k+1}, \psi_{l+1,k+2}, \psi_{l+2,k-1}, \psi_{l+2,k}, \psi_{l+2,k+1}, \psi_{l+2,k+2}]^T. \end{aligned}$$

The element matrices $A^e_{(n,m),(i,j)}$, $B^e_{(n,m),(i,j)}$, and $D^e_{(n,m),(i,j)}$ are given by

$$\begin{aligned} A^e_{(n,m),(i,j)} = D^e_{(n,m),(i,j)} &= \int_0^{h_x}\int_0^{h_y} B_{n,m}(\mu,\eta)\, B_{i,j}(\mu,\eta)\, d\mu\, d\eta, \\ B^e_{(n,m),(i,j)} &= \int_0^{h_x}\int_0^{h_y} \nabla B_{n,m}(\mu,\eta)\cdot\nabla B_{i,j}(\mu,\eta)\, d\mu\, d\eta. \end{aligned} \tag{2.17}$$

Here, the indices $n, i \in \{l-1, l, l+1, l+2\}$ and $m, j \in \{k-1, k, k+1, k+2\}$ correspond to the local bicubic B-spline basis functions that are nonzero over the element $[x_l, x_{l+1}] \times [y_k, y_{k+1}]$. As a result, the element matrices A^e, B^e, and D^e are of size 16×16 and can be obtained as follows:

$$A^e_{(n,m),(i,j)} = D^e_{(n,m),(i,j)} = \int_0^{h_x}\int_0^{h_y} B_{n,m}(\mu,\eta)\, B_{i,j}(\mu,\eta)\, d\mu\, d\eta = \frac{h_x h_y}{19600} A^e \tag{2.18}$$

with

$$A^e = \begin{bmatrix} A^e_{1,1} & A^e_{1,2} & A^e_{1,3} & A^e_{1,4} \\ A^e_{2,1} & A^e_{2,2} & A^e_{2,3} & A^e_{2,4} \\ A^e_{3,1} & A^e_{3,2} & A^e_{3,3} & A^e_{3,4} \\ A^e_{4,1} & A^e_{4,2} & A^e_{4,3} & A^e_{4,4} \end{bmatrix}, \qquad A^e_{\alpha,\gamma} \in \mathbb{R}^{4\times 4},$$

where $A^e_{\alpha,\gamma}$ $(\alpha, \gamma = 1, 2, 3, 4)$ denotes the 4×4 block submatrices of the element mass matrix A^e. Owing to symmetry, several blocks are identical and are given as follows:

$$A^e_{1,1} = A^e_{4,4} = \begin{bmatrix} 400 & 2580 & 1200 & 20 \\ 2580 & 23760 & 18660 & 1200 \\ 1200 & 18660 & 23760 & 2580 \\ 20 & 1200 & 2580 & 400 \end{bmatrix},$$

$$A^e_{1,2} = A^e_{2,1} = A^e_{3,4} = A^e_{4,3} = \begin{bmatrix} 2580 & 16641 & 7740 & 129 \\ 16641 & 153252 & 120357 & 7740 \\ 7740 & 120357 & 153252 & 16641 \\ 129 & 7740 & 16641 & 2580 \end{bmatrix},$$

$$A^e_{1,3} = A^e_{2,4} = A^e_{3,1} = A^e_{4,2} = \begin{bmatrix} 1200 & 7740 & 3600 & 60 \\ 7740 & 71280 & 55980 & 3600 \\ 3600 & 55980 & 71280 & 7740 \\ 60 & 3600 & 7740 & 1200 \end{bmatrix},$$

$$A^e_{1,4} = A^e_{4,1} = \begin{bmatrix} 20 & 129 & 60 & 1 \\ 129 & 1188 & 933 & 60 \\ 60 & 933 & 1188 & 129 \\ 1 & 60 & 129 & 20 \end{bmatrix},$$

$$A^e_{2,2} = A^e_{3,3} = \begin{bmatrix} 23760 & 153252 & 71280 & 1188 \\ 153252 & 1411344 & 1108404 & 71280 \\ 71280 & 1108404 & 1411344 & 153252 \\ 1188 & 71280 & 153252 & 23760 \end{bmatrix},$$

$$A^e_{2,3} = A^e_{3,2} = \begin{bmatrix} 18660 & 120357 & 55980 & 933 \\ 120357 & 1108404 & 870489 & 55980 \\ 55980 & 870489 & 1108404 & 120357 \\ 933 & 55980 & 120357 & 18660 \end{bmatrix}.$$

All other block entries follow by symmetry. Similar calculations can be done to the element matrix $B^e_{(n,m),(i,j)}$:

$$B^e_{(n,m),(i,j)} = \int_0^{h_x}\int_0^{h_y} \nabla B_{n,m}(\mu,\eta)\cdot\nabla B_{i,j}(\mu,\eta)\, d\mu, d\eta = \frac{3}{1400\, h_x h_y}\, B^e. \tag{2.19}$$

$$B^e = \begin{bmatrix} B^e_{1,1} & B^e_{1,2} & B^e_{1,3} & B^e_{1,4} \\ B^e_{2,1} & B^e_{2,2} & B^e_{2,3} & B^e_{2,4} \\ B^e_{3,1} & B^e_{3,2} & B^e_{3,3} & B^e_{3,4} \\ B^e_{4,1} & B^e_{4,2} & B^e_{4,3} & B^e_{4,4} \end{bmatrix}, \qquad B^e_{\alpha,\gamma} \in \mathbb{R}^{4\times 4}.$$

Due to symmetry of the bicubic B-spline basis, several block of submatrices are identical. The distinct 4×4 blocks are listed as follows:

$$B^e_{1,1} = B^e_{4,4} = \begin{bmatrix} 120(h_x^2+h_y^2) & 140h_x^2+774h_y^2 & 360h_y^2-240h_x^2 & 6h_y^2-20h_x^2 \\ 140h_x^2+774h_y^2 & 680h_x^2+7128h_y^2 & 5598h_y^2-580h_x^2 & 360h_y^2-240h_x^2 \\ 360h_y^2-240h_x^2 & 5598h_y^2-580h_x^2 & 680h_x^2+7128h_y^2 & 140h_x^2+774h_y^2 \\ 6h_y^2-20h_x^2 & 360h_y^2-240h_x^2 & 140h_x^2+774h_y^2 & 120(h_x^2+h_y^2) \end{bmatrix},$$

$$\begin{aligned} B^e_{1,2} &= B^e_{2,1} = B^e_{3,4} = B^e_{4,3} \\ &= \begin{bmatrix} 774h_x^2+140h_y^2 & 903(h_x^2+h_y^2) & 420h_y^2-1548h_x^2 & 7h_y^2-129h_x^2 \\ 903(h_x^2+h_y^2) & 4386h_x^2+8316h_y^2 & 6531h_y^2-3741h_x^2 & 420h_y^2-1548h_x^2 \\ 420h_y^2-1548h_x^2 & 6531h_y^2-3741h_x^2 & 4386h_x^2+8316h_y^2 & 903(h_x^2+h_y^2) \\ 7h_y^2-129h_x^2 & 420h_y^2-1548h_x^2 & 903(h_x^2+h_y^2) & 774h_x^2+140h_y^2 \end{bmatrix}, \end{aligned}$$

$$\begin{aligned} B^e_{1,3} &= B^e_{2,4} = B^e_{3,1} = B^e_{4,2} \\ &= \begin{bmatrix} 360h_x^2-240h_y^2 & 420h_x^2-1548h_y^2 & -720(h_x^2+h_y^2) & -12(5h_x^2+h_y^2) \\ 420h_x^2-1548h_y^2 & 2040h_x^2-14256h_y^2 & -12(145h_x^2+933h_y^2) & -720(h_x^2+h_y^2) \\ -720(h_x^2+h_y^2) & -12(145h_x^2+933h_y^2) & 2040h_x^2-14256h_y^2 & 420h_x^2-1548h_y^2 \\ -12(5h_x^2+h_y^2) & -720(h_x^2+h_y^2) & 420h_x^2-1548h_y^2 & 360h_x^2-240h_y^2 \end{bmatrix}, \end{aligned}$$

$$B^e_{1,4} = B^e_{4,1} = \begin{bmatrix} 6h_x^2-20h_y^2 & 7h_x^2-129h_y^2 & -12(h_x^2+5h_y^2) & -(h_x^2+h_y^2) \\ 7h_x^2-129h_y^2 & 34h_x^2-1188h_y^2 & -(29h_x^2+933h_y^2) & -12(h_x^2+5h_y^2) \\ -12(h_x^2+5h_y^2) & -(29h_x^2+933h_y^2) & 34h_x^2-1188h_y^2 & 7h_x^2-129h_y^2 \\ -(h_x^2+h_y^2) & -12(h_x^2+5h_y^2) & 7h_x^2-129h_y^2 & 6h_x^2-20h_y^2 \end{bmatrix},$$

$$\begin{aligned} B^e_{2,2} &= B^e_{3,3} \\ &= \begin{bmatrix} 7128h_x^2+680h_y^2 & 8316h_x^2+4386h_y^2 & 2040h_y^2-14256h_x^2 & 34h_y^2-1188h_x^2 \\ 8316h_x^2+4386h_y^2 & 40392(h_x^2+5h_y^2) & 31722h_y^2-34452h_x^2 & 2040h_y^2-14256h_x^2 \\ 2040h_y^2-14256h_x^2 & 31722h_y^2-34452h_x^2 & 40392(h_x^2+5h_y^2) & 8316h_x^2+4386h_y^2 \\ 34h_y^2-1188h_x^2 & 2040h_y^2-14256h_x^2 & 8316h_x^2+4386h_y^2 & 7128h_x^2+680h_y^2 \end{bmatrix}, \end{aligned}$$

$$
\begin{aligned}
B^e_{12} &= B^e_{21}\\
&= \begin{bmatrix}
5598h_x^2 - 580h_y^2 & 6531h_x^2 - 3741h_y^2 & -12(145h_x^2 + 933h_y^2) & -(933h_x^2 + 29h_y^2)\\
6531h_x^2 - 3741h_y^2 & 31722h_x^2 - 34452h_y^2 & -27057(h_x^2 + h_y^2) & -12(145h_x^2 + 933h_y^2)\\
-12(145h_x^2 + 933h_y^2) & -27057(h_x^2 + h_y^2) & 31722h_x^2 - 34452h_y^2 & 6531h_x^2 - 3741h_y^2\\
-(933h_x^2 + 29h_y^2) & -12(145h_x^2 + 933h_y^2) & 6531h_x^2 - 3741h_y^2 & 5598h_x^2 - 580h_y^2
\end{bmatrix}.
\end{aligned}
$$

The nonlinear coefficient is approximated element-wise by evaluating r and s at the center of the element. Specifically, it can be defined as

$$
r^e_{l,k} = \frac{1}{4}(r_{l,k} + r_{l+1,k} + r_{l,k+1} + r_{l+1,k+1}), \qquad s^e_{l,k} = \frac{1}{4}(s_{l,k} + s_{l+1,k} + s_{l,k+1} + s_{l+1,k+1}).
$$

Accordingly, the nonlinear coefficient is approximated as

$$
\begin{aligned}
z_{l,k} = \tfrac{q}{16} \Big[&(\rho_{l-1,k-1} + 5\rho_{l-1,k} + 5\rho_{l-1,k+1} + \rho_{l-1,k+2} + 5\rho_{l,k-1} + 25\rho_{l,k} + 25\rho_{l,k+1}\\
&+5\rho_{l,k+2} + 5\rho_{l+1,k-1} + 25\rho_{l+1,k} + 25\rho_{l+1,k+1} + 5\rho_{l+1,k+2} + \rho_{l+2,k-1} + 5\rho_{l+2,k}\\
&+5\rho_{l+2,k+1} + \rho_{l+2,k+2})^2 + (\psi_{l-1,k-1} + 5\psi_{l-1,k} + 5\psi_{l-1,k+1} + \psi_{l-1,k+2}\\
&+5\psi_{l,k-1} + 25\psi_{l,k} + 25\psi_{l,k+1} + 5\psi_{l,k+2} + 5\psi_{l+1,k-1} + 25\psi_{l+1,k}\\
&+25\psi_{l+1,k+1} + 5\psi_{l+1,k+2} + \psi_{l+2,k-1} + 5\psi_{l+2,k} + 5\psi_{l+2,k+1} + \psi_{l+2,k+2})^2 \Big].
\end{aligned} \tag{2.20}
$$

By assembling the element contributions over all elements and enforcing the periodic boundary conditions, the semi-discrete system (2.16) leads to a global system of ordinary differential equations of the form:

$$
\begin{aligned}
A\,\dot{\boldsymbol{\psi}} + B\,\boldsymbol{\rho} - D(\mathbf{z})\,\boldsymbol{\rho} &= \mathbf{0},\\
A\,\dot{\boldsymbol{\rho}} - B\,\boldsymbol{\psi} + D(\mathbf{z})\,\boldsymbol{\psi} &= \mathbf{0}.
\end{aligned} \tag{2.21}
$$

Here, $\boldsymbol{\rho}(t)$ and $\boldsymbol{\psi}(t)$ denote the global vectors of time-dependent spline coefficients associated with the numerical solution in its real and imaginary parts, respectively, where

$$
\begin{aligned}
\rho = [&\rho_{-1,-1}, \ldots, \rho_{-1,M+1}, \rho_{0,-1}, \ldots, \rho_{0,M+1}, \ldots, \rho_{N,-1},\\
&\ldots, \rho_{N,M+1}, \rho_{N+1,-1}, \ldots, \rho_{N+1,M+1}]^T
\end{aligned}
$$

and

$$
\begin{aligned}
\psi = [&\psi_{-1,-1}, \ldots, \psi_{-1,M+1}, \psi_{0,-1}, \ldots, \psi_{0,M+1}, \ldots, \psi_{N,-1},\\
&\ldots, \psi_{N,M+1}, \psi_{N+1,-1}, \ldots, \psi_{N+1,M+1}]^T.
\end{aligned}
$$

The matrices A and B denote the assembled global mass and stiffness matrices, respectively, whereas $D(\mathbf{z})$ denotes the assembled nonlinear weighted mass matrix associated with the element-wise nonlinear coefficient $z_{l,k}$. The periodic boundary conditions are incorporated during the assembly by identifying the corresponding degrees of freedom on opposite boundaries. Consequently, the global matrices A, B, and $D(\mathbf{z})$ admit sparse septa-diagonal block structures with periodic wrap-around, and the kth row of each block matrix can be written in the following form:

$$
A = \frac{h_x h_y}{19600} \begin{pmatrix} A_1 & A_2 & A_3 & A_4 & A_5 & A_6 & A_7 \end{pmatrix}, \tag{2.22}
$$

where

$$A_1 = A_7 = (1,\ 120,\ 1191,\ 2416,\ 1191,\ 120,\ 1),$$
$$A_2 = A_6 = (120,\ 14400,\ 142920,\ 289920,\ 142920,\ 14400,\ 120),$$
$$A_3 = A_5 = (1191,\ 142920,\ 1418481,\ 2877456,\ 1418481,\ 142920,\ 1191),$$
$$A_4 = (2416,\ 289920,\ 2877456,\ 5837056,\ 2877456,\ 289920,\ 2416),$$

$$B = \frac{3}{1400\, h_x h_y}\begin{pmatrix} B_1 & B_2 & B_3 & B_4 & B_5 & B_6 & B_7 \end{pmatrix}, \tag{2.23}$$

where

$$\begin{aligned} B_1 = B_7 = (&-(h_x^2+h_y^2),\ -24h_x^2-120h_y^2,\ -15h_x^2-1191h_y^2,\ 80h_x^2-2416h_y^2,\\ &-15h_x^2-1191h_y^2,\ -24h_x^2-120h_y^2,\ -(h_x^2+h_y^2)),\end{aligned}$$

$$\begin{aligned} B_2 = B_6 = (&-24h_x^2-120h_y^2,\ -2880h_x^2-2880h_y^2,\ -1800h_x^2-28584h_y^2,\ 9600h_x^2-57984h_y^2,\\ &-1800h_x^2-28584h_y^2,\ -2880h_x^2-2880h_y^2,\ -24h_x^2-120h_y^2),\end{aligned}$$

$$\begin{aligned} B_3 = B_5 = (&-15h_y^2-1191h_x^2,\ -1800h_y^2-28584h_x^2,\ -17865(h_x^2+h_y^2),\\ &95280h_x^2-36240h_y^2,\ -17865(h_x^2+h_y^2),\ -1800h_y^2-28584h_x^2,\ -15h_y^2-1191h_x^2),\end{aligned}$$

$$\begin{aligned} B_4 = (&80h_y^2-2416h_x^2,\ 9600h_y^2-57984h_x^2,\ 95280h_y^2-36240h_x^2,\\ &193280(h_x^2+h_y^2),\ 95280h_y^2-36240h_x^2,\ 9600h_y^2-57984h_x^2,\ 80h_y^2-2416h_x^2),\end{aligned}$$

and

$$D(z_{l,k}) = \frac{h_x h_y}{19600}\begin{pmatrix} D_1(z_{l,k}) & D_2(z_{l,k}) & D_3(z_{l,k}) & D_4(z_{l,k}) & D_5(z_{l,k}) & D_6(z_{l,k}) & D_7(z_{l,k}) \end{pmatrix}, \tag{2.24}$$

where

$$\begin{aligned} D_1(z_{l,k}) = (&z_{1l,1k}, 60z_{1l,1k}+60z_{1l,2k}, 129z_{1l,1k}+933z_{1l,2k}+129z_{1l,3k}, 20z_{1l,1k}\\ &+1188z_{1l,2k}+1188z_{1l,3k}+20z_{1l,4k}, 129z_{1l,2k}+933z_{1l,3k}\\ &+129z_{1l,4k}, 60z_{1l,3k}+60z_{1l,4k}, z_{1l,4k}),\end{aligned}$$

$$\begin{aligned} D_2(z_{l,k}) = (&60z_{1l,1k}+60z_{2l,1k}, 3600z_{1l,1k}+3600z_{2l,1k}+3600z_{1l,2k}+3600z_{2l,2k}, 7740z_{1l,1k}\\ &+7740z_{2l,1k}+55980z_{1l,2k}+55980z_{2l,2k}+7740z_{1l,3k}+7740z_{2l,3k}, 1200z_{1l,1k}\\ &+1200z_{21,1k}+71280z_{1l,2k}+71280z_{2l,2k}+71280z_{1l,3k}+71280z_{2l,3k}\\ &+1200z_{1l,4k}+1200z_{2l,4k}, 7740z_{1l,2k}+7740z_{2l,2k}+55980z_{1l,3k}+55980z_{2l,3k}\\ &+7740z_{1l,4k}+7740z_{2l,4k}, 3600z_{1l,3k}+3600z_{2l,3k}\\ &+3600z_{1l,4k}+3600z_{2l,4k}, 60z_{1l,4k}+60z_{2l,4k}),\end{aligned}$$

$$\begin{aligned} D_3(z_{l,k}) = (&129z_{1l,1k}+933z_{2l,1k}+129z_{3l,1k}, 7740z_{1l,1k}+7740z_{2l,1k}+55980z_{3l,1k}\\ &+55980z_{1l,2k}+7740z_{2l,2k}+7740z_{3l,2k}, 16641z_{1l,1k}+120357z_{2l,1k}\\ &+16641z_{3l,1k}+120357z_{1l,2k}+870489z_{2l,2k}+120357z_{3l,2k}+16641z_{1l,3k}\\ &+120357z_{2l,3k}+16641z_{3l,3k}, 2580z_{1l,1k}+18660z_{2l,1k}+2580z_{3l,1k}\\ &+153252z_{1l,2k}+1108404z_{2l,2k}+153252z_{3l,2k}+153252z_{1l,3k}\\ &+1108404z_{2l,3k}+153252z_{3l,3k}+2580z_{1l,4k}+18660z_{2l,4k}+2580z_{3l,4k}, 16641z_{1l,2k}\end{aligned}$$

$$+ 120357z_{2l,2k} + 16641z_{3l,2k} + 120357z_{1l,3k} + 870489z_{2l,3k}$$
$$+ 120357z_{3l,3k} + 16641z_{1l,4k} + 120357z_{2l,4k} + 16641z_{3l,4k}, 7740z_{1l,3k}$$
$$+ 7740z_{2l,3k} + 55980z_{3l,3k} + 55980z_{1l,4k} + 7740z_{2l,4k} + 7740z_{3l,4k}, 129z_{1l,4k}$$
$$+ 933z_{2l,4k} +129z_{3l,4k}),$$

$$\begin{aligned}
D_4(z_{l,k}) = (&20z_{1l,1k} + 1188z_{2l,1k} + 1188z_{3l,1k} + 20z_{4l,1k}, 1200z_{1l,1k}+71280z_{2l,1k}\\
&+71280z_{3l,1k}+1200z_{4l,1k}+1200z_{1l,2k}+71280z_{2l,2k}+71280z_{3l,2k}+1200z_{4l,2k}, 2580z_{1l,1k}\\
&+153252z_{2l,1k}+153252z_{3l,1k}+2580z_{4l,1k}+18660z_{1l,2k}\\
&+1108404z_{2l,2k}+1108404z_{3l,2k}+18660z_{4l,2k}+2580z_{1l,3k}\\
&+153252z_{2l,3k}+153252z_{3l,3k}+2580z_{4l,3k}, 400z_{1l,1k}+23760z_{2l,1k}\\
&+23760z_{3l,1k}+400z_{4l,1k}+23760z_{1l,2k}+1411344z_{2l,2k}+1411344z_{3l,2k}\\
&+23760z_{4l,2k}+23760z_{1l,3k}+1411344z_{2l,3k}+1411344z_{3l,3k}+23760z_{4l,3k}\\
&+400z_{1l,4k}+23760z_{2l,4k}+23760z_{3l,4k}+400z_{4l,4k}, 2580z_{1l,2k}\\
&+153252z_{2l,2k}+153252z_{3l,2k}+2580z_{4l,2k}+18660z_{1l,3k}+1108404z_{2l,3k}\\
&+1108404z_{3l,3k}+18660z_{4l,3k}+2580z_{1l,4k}+153252z_{2L,4k}+153252z_{3l,4k}\\
&+2580z_{4l,4k}, 1200z_{1l,3k}+71280z_{2l,3k}+71280z_{3l,3k}+1200z_{4l,3k}\\
&+1200z_{1l,4k}+71280z_{2l,4k}+71280z_{3l,4k}+1200z_{4l,4k}, 20z_{1l,4k}+1188z_{2l,4k}\\
&+1188z_{3l,4k}+ 20z_{4l,4k}),
\end{aligned}$$

$$\begin{aligned}
D_5(z_{l,k}) = (&129z_{2l,1k} + 933z_{3l,1k}+129z_{4l,1k}, 7740z_{2l,1k}+55980z_{3l,1k}+7740z_{4l,1k}\\
&+7740z_{2l,2k}+55980z_{3l,2k}+7740z_{4l,2k}, 16641z_{2l,1k}+120357z_{3l,1k}\\
&+16641z_{4l,1k}+120357z_{2l,2k}+870489z_{3l,2k}+120357z_{4l,2k}+16641z_{2l,3k}\\
&+120357z_{3l,3k}+16641z_{4l,3k}, 2580z_{2l,1k}+18660z_{3l,1k}+2580z_{4l,1k}\\
&+153252z_{2l,2k}+1108404z_{3l,2k}+153252z_{4l,2k}+153252z_{2l,3k}\\
&+1108404z_{3l,3k}+153252z_{4l,3k}+2580z_{2l,4k}+18660z_{3l,4w}+2580z_{4l,4k}, 16641z_{2l,2k}\\
&+120357z_{3l,2k}+16641z_{4l,2k}+120357z_{2l,3k}+870489z_{3l,3k}\\
&+120357z_{4l,3k}+16641z_{2l,4k}+120357z_{3l,4k}+16641z_{4l,4k}, 7740z_{2l,3k}\\
&+55980z_{3l,3k}+7740z_{4l,3k}+7740z_{2l,4k}+55980z_{3l,4k}+7740z_{4l,4k}, 129z_{2l,4k}\\
&+933z_{3l,4k}+ 129z_{4l,4k}),
\end{aligned}$$

$$\begin{aligned}
D_6(z_{l,k}) = (&60z_{3l,1k} +60z_{4l,1k}, 3600z_{3l,1k}+3600z_{4l,1k}+3600z_{3l,2k}+3600z_{4l,2k}, 7740z_{3l,1k}\\
&+7740z_{4l,1k}+55980z_{3l,2k}+55980z_{4l,2k}+7740z_{3l,3k}\\
&+7740z_{4l,3k}, 1200z_{3l,1k}+1200z_{4l,1k}+71280z_{3l,2k}+71280z_{4l,2k}\\
&+71280z_{3l,3k}+71280z_{4l,3k}+1200z_{3l,4k}+1200z_{4l,4k}, 7740z_{3l,2k}\\
&+7740z_{4l,2k}+55980z_{3l,3k}+55980z_{4l,3k}+7740z_{3l,4k}+7740z_{4l,4k}, 3600z_{3l,3k}\\
&+3600z_{4l,3k}+3600z_{3l,4k}+3600z_{4l,4k}, 60z_{3l,4k}+ 60z_{4l,4k}),
\end{aligned}$$

$$
\begin{aligned}
D_7(z_{l,k}) = (&z_{4l,1k}\ , 60z_{4l,1k} + 60z_{4l,2k}, 129z_{4l,1k} + 933z_{4l,2k} + 129z_{4l,3k}, 20z_{4l,1k} \\
&+ 1188z_{4l,2k} + 1188z_{4l,3k} + 20z_{4l,4k}, 129z_{4l,2k} + 933z_{4l,3k} \\
&+ 129z_{4l,4k}, 60z_{4l,3k} + 60z_{4l,4k}, z_{4l,4k})\,,
\end{aligned} \tag{2.25}
$$

where

$$
\begin{aligned}
z_{1l,1k} =& \frac{q}{16}\Big[(\rho_{l-2,k-2} + 5\rho_{l-2,k-1} + 5\rho_{l-2,k} + \rho_{l-2,k+1} + 5\rho_{l-1,k-2} + 25\rho_{l-1,k-1} \\
&+ 25\rho_{l-1,k} + 5\rho_{l-1,k+1} + 5\rho_{l,k-2} + 25\rho_{l,k-1} + 25\rho_{l,k} + 5\rho_{l,k+1} \\
&+ \rho_{l+1,k-2} + 5\rho_{l+1,k-1} + 5\rho_{l+1,k} + \rho_{l+1,k+1})^2 + (\psi_{l-2,k-2} \\
&+ 5\psi_{l-2,k-1} + 5\psi_{l-2,k} + \psi_{l-2,k+1} + 5\psi_{l-1,k-2} + 25\psi_{l-1,k-1} + 25\psi_{l-1,k} \\
&+ 5\psi_{l-1,k+1} + 5\psi_{l,k-2} + 25\psi_{l,k-1} + 25\psi_{l,k} + 5\psi_{l,k+1} + \psi_{l+1,k-2} \\
&+ 5\psi_{l+1,k-1} + 5\psi_{l+1,k} + \psi_{l+1,k+1})^2\Big],
\end{aligned}
$$

$$
\begin{aligned}
z_{1l,2k} =& \frac{q}{16}\Big[(\rho_{l-2,k-1} + 5\rho_{l-2,k} + 5\rho_{l-2,k+1} + \rho_{l-2,k+2} + 5\rho_{l-1,k-1} + 25\rho_{l-1,k} \\
&+ 25\rho_{l-1,k+1} + 5\rho_{l-1,k+2} + 5\rho_{l,k-1} + 25\rho_{l,k} + 25\rho_{l,k+1} + 5\rho_{l,k+2} \\
&+ \rho_{l+1,k-1} + 5\rho_{l+1,k} + 5\rho_{l+1,k+1} + \rho_{l+1,k+2})^2 + (\psi_{l-2,k-1} \\
&+ 5\psi_{l-2,k} + 5\psi_{l-2,k+1} + \psi_{l-2,k+2} + 5\psi_{l-1,k-1} + 25\psi_{l-1,k} + 25\psi_{l-1,k+1} \\
&+ 5\psi_{l-1,k+2} + 5\psi_{l,k-1} + 25\psi_{l,k} + 25\psi_{l,k+1} + 5\psi_{l,k+2} + \psi_{l+1,k-1} \\
&+ 5\psi_{l+1,k} + 5\psi_{l+1,k+1} + \psi_{l+1,k+2})^2\Big],
\end{aligned}
$$

$$
\begin{aligned}
z_{1l,3k} =& \frac{q}{16}\Big[(\rho_{l-2,k} + 5\rho_{l-2,k+1} + 5\rho_{l-2,k+2} + \rho_{l-2,k+3} + 5\rho_{l-1,k} + 25\rho_{l-1,k+1} \\
&+ 25\rho_{l-1,k+2} + 5\rho_{l-1,k+3} + 5\rho_{l,k} + 25\rho_{l,k+1} + 25\rho_{l,k+2} + 5\rho_{l,k+3} \\
&+ \rho_{l+1,k} + 5\rho_{l+1,k+1} + 5\rho_{l+1,k+2} + \rho_{l+1,k+3})^2 + (\psi_{l-2,k} + 5\psi_{l-2,k+1} \\
&+ 5\psi_{l-2,k+2} + \psi_{l-2,k+3} + 5\psi_{l-1,k} + 25\psi_{l-1,k+1} + 25\psi_{l-1,k+2} \\
&+ 5\psi_{l-1,k+3} + 5\psi_{l,k} + 25\psi_{l,k+1} + 25\psi_{l,k+2} + 5\psi_{l,k+3} + \psi_{l+1,k} \\
&+ 5\psi_{l+1,k+1} + 5\psi_{l+1,k+2} + \psi_{l+1,k+3})^2\Big],
\end{aligned}
$$

$$
\begin{aligned}
z_{1l,4k} =& \frac{q}{16}\Big[(\rho_{l-2,k+1} + 5\rho_{l-2,k+2} + 5\rho_{l-2,k+3} + \rho_{l-2,k+4} + 5\rho_{l-1,k+1} + 25\rho_{l-1,k+2} \\
&+ 25\rho_{l-1,k+3} + 5\rho_{l-1,k+4} + 5\rho_{l,k+1} + 25\rho_{l,k+2} + 25\rho_{l,k+3} + 5\rho_{l,k+4} \\
&+ \rho_{l+1,k+1} + 5\rho_{l+1,k+2} + 5\rho_{l+1,k+3} + \rho_{l+1,k+4})^2 + (\psi_{l-2,k+1} + 5\psi_{l-2,k+2} \\
&+ 5\psi_{l-2,k+3} + \psi_{l-2,k+4} + 5\psi_{l-1,k+1} + 25\psi_{l-1,k+2} + 25\psi_{l-1,k+3} \\
&+ 5\psi_{l-1,k+4} + 5\psi_{l,k+1} + 25\psi_{l,k+2} + 25\psi_{l,k+3} + 5\psi_{l,k+4} + \psi_{l+1,k+1} \\
&+ 5\psi_{l+1,k+2} + 5\psi_{l+1,k+3} + \psi_{l+1,k+4})^2\Big],
\end{aligned}
$$

$$
z_{2l,1k} = \frac{q}{16}\Big[(\rho_{l-1,k-2} + 5\rho_{l-1,k-1} + 5\rho_{l-1,k} + \rho_{l-1,k+1} + 5\rho_{l,k-2} + 25\rho_{l,k-1}
$$

$$+ 25\rho_{l,k} + 5\rho_{l,k+1} + 5\rho_{l+1,k-2} + 25\rho_{l+1,k-1} + 25\rho_{l+1,k} + 5\rho_{l+1,k+1}$$
$$+ \rho_{l+2,k-2} + 5\rho_{l+2,k-1} + 5\rho_{l+2,k} + \rho_{l+2,k+1})^2 + (\psi_{l-1,k-2} + 5\psi_{l-1,k-1}$$
$$+ 5\psi_{l-1,k} + \psi_{l-1,k+1} + 5\psi_{l,k-2} + 25\psi_{l,k-1} + 25\psi_{l,k} + 5\psi_{l,k+1}$$
$$+ 5\psi_{l+1,k-2} + 25\psi_{l+1,k-1} + 25\psi_{l+1,k} + 5\psi_{l+1,k+1} + \psi_{l+2,k-2}$$
$$+ 5\psi_{l+2,k-1} + 5\psi_{l+2,k} + \psi_{l+2,k+1})^2\Big],$$

$$z_{2l,2k} = \frac{q}{16}\Big[(\rho_{l-1,k-1} + 5\rho_{l-1,k} + 5\rho_{l-1,k+1} + \rho_{l-1,k+2} + 5\rho_{l,k-1} + 25\rho_{l,k}$$
$$+ 25\rho_{l,k+1} + 5\rho_{l,k+2} + 5\rho_{l+1,k-1} + 25\rho_{l+1,k} + 25\rho_{l+1,k+1} + 5\rho_{l+1,k+2}$$
$$+ \rho_{l+2,k-1} + 5\rho_{l+2,k} + 5\rho_{l+2,k+1} + \rho_{l+2,k+2})^2 + (\psi_{l-1,k-1} + 5\psi_{l-1,k}$$
$$+ 5\psi_{l-1,k+1} + \psi_{l-1,k+2} + 5\psi_{l,k-1} + 25\psi_{l,k} + 25\psi_{l,k+1} + 5\psi_{l,k+2}$$
$$+ 5\psi_{l+1,k-1} + 25\psi_{l+1,k} + 25\psi_{l+1,k+1} + 5\psi_{l+1,k+2} + \psi_{l+2,k-1}$$
$$+ 5\psi_{l+2,k} + 5\psi_{l+2,k+1} + \psi_{l+2,k+2})^2\Big],$$

$$z_{2l,3k} = \frac{q}{16}\Big[(\rho_{l-1,k} + 5\rho_{l-1,k+1} + 5\rho_{l-1,k+2} + \rho_{l-1,k+3} + 5\rho_{l,k} + 25\rho_{l,k+1}$$
$$+ 25\rho_{l,k+2} + 5\rho_{l,k+3} + 5\rho_{l+1,k} + 25\rho_{l+1,k+1} + 25\rho_{l+1,k+2} + 5\rho_{l+1,k+3}$$
$$+ \rho_{l+2,k} + 5\rho_{l+2,k+1} + 5\rho_{l+2,k+2} + \rho_{l+2,k+3})^2 + (\psi_{l-1,k} + 5\psi_{l-1,k+1}$$
$$+ 5\psi_{l-1,k+2} + \psi_{l-1,k+3} + 5\psi_{l,k} + 25\psi_{l,k+1} + 25\psi_{l,k+2} + 5\psi_{l,k+3}$$
$$+ 5\psi_{l+1,k} + 25\psi_{l+1,k+1} + 25\psi_{l+1,k+2} + 5\psi_{l+1,k+3} + \psi_{l+2,k}$$
$$+ 5\psi_{l+2,k+1} + 5\psi_{l+2,k+2} + \psi_{l+2,k+3})^2\Big],$$

$$z_{2l,4k} = \frac{q}{16}\Big[(\rho_{l-1,k+1} + 5\rho_{l-1,k+2} + 5\rho_{l-1,k+3} + \rho_{l-1,k+4} + 5\rho_{l,k+1} + 25\rho_{l,k+2}$$
$$+ 25\rho_{l,k+3} + 5\rho_{l,k+4} + 5\rho_{l+1,k+1} + 25\rho_{l+1,k+2} + 25\rho_{l+1,k+3} + 5\rho_{l+1,k+4}$$
$$+ \rho_{l+2,k+1} + 5\rho_{l+2,k+2} + 5\rho_{l+2,k+3} + \rho_{l+2,k+4})^2 + (\psi_{l-1,k+1} + 5\psi_{l-1,k+2}$$
$$+ 5\psi_{l-1,k+3} + \psi_{l-1,k+4} + 5\psi_{l,k+1} + 25\psi_{l,k+2} + 25\psi_{l,k+3} + 5\psi_{l,k+4}$$
$$+ 5\psi_{l+1,k+1} + 25\psi_{l+1,k+2} + 25\psi_{l+1,k+3} + 5\psi_{l+1,k+4} + \psi_{l+2,k+1}$$
$$+ 5\psi_{l+2,k+2} + 5\psi_{l+2,k+3} + \psi_{l+2,k+4})^2\Big],$$

$$z_{3l,1k} = \frac{q}{16}\Big[(\rho_{l,k-2} + 5\rho_{l,k-1} + 5\rho_{l,k} + \rho_{l,k+1} + 5\rho_{l+1,k-2} + 25\rho_{l+1,k-1} + 25\rho_{l+1,k}$$
$$+ 5\rho_{l+1,k+1} + 5\rho_{l+2,k-2} + 25\rho_{l+2,k-1} + 25\rho_{l+2,k} + 5\rho_{l+2,k+1} + \rho_{l+3,k-2}$$
$$+ 5\rho_{l+3,k-1} + 5\rho_{l+3,k} + \rho_{l+3,k+1})^2 + (\psi_{l,k-2} + 5\psi_{l,k-1} + 5\psi_{l,k} + \psi_{l,k+1}$$
$$+ 5\psi_{l+1,k-2} + 25\psi_{l+1,k-1} + 25\psi_{l+1,k} + 5\psi_{l+1,k+1} + 5\psi_{l+2,k-2} + 25\psi_{l+2,k-1}$$
$$+ 25\psi_{l+2,k} + 5\psi_{l+2,k+1} + \psi_{l+3,k-2} + 5\psi_{l+3,k-1} + 5\psi_{l+3,k} + \psi_{l+3,k+1})^2\Big],$$

$$
\begin{aligned}
z_{3l,2k} = \frac{q}{16} \Big[& (\rho_{l,k-1} + 5\rho_{l,k} + 5\rho_{l,k+1} + \rho_{l,k+2} + 5\rho_{l+1,k-1} + 25\rho_{l+1,k} + 25\rho_{l+1,k+1} \\
& + 5\rho_{l+1,k+2} + 5\rho_{l+2,k-1} + 25\rho_{l+2,k} + 25\rho_{l+2,k+1} + 5\rho_{l+2,k+2} + \rho_{l+3,k-1} \\
& + 5\rho_{l+3,k} + 5\rho_{l+3,k+1} + \rho_{l+3,k+2})^2 + (\psi_{l,k-1} + 5\psi_{l,k} + 5\psi_{l,k+1} + \psi_{l,k+2} \\
& + 5\psi_{l+1,k-1} + 25\psi_{l+1,k} + 25\psi_{l+1,k+1} + 5\psi_{l+1,k+2} + 5\psi_{l+2,k-1} + 25\psi_{l+2,k} \\
& + 25\psi_{l+2,k+1} + 5\psi_{l+2,k+2} + \psi_{l+3,k-1} + 5\psi_{l+3,k} + 5\psi_{l+3,k+1} + \psi_{l+3,k+2})^2 \Big],
\end{aligned}
$$

$$
\begin{aligned}
z_{3l,3k} = \frac{q}{16} \Big[& (\rho_{l,k} + 5\rho_{l,k+1} + 5\rho_{l,k+2} + \rho_{l,k+3} + 5\rho_{l+1,k} + 25\rho_{l+1,k+1} + 25\rho_{l+1,k+2} \\
& + 5\rho_{l+1,k+3} + 5\rho_{l+2,k} + 25\rho_{l+2,k+1} + 25\rho_{l+2,k+2} + 5\rho_{l+2,k+3} + \rho_{l+3,k} \\
& + 5\rho_{l+3,k+1} + 5\rho_{l+3,k+2} + \rho_{l+3,k+3})^2 + (\psi_{l,k} + 5\psi_{l,k+1} + 5\psi_{l,k+2} + \psi_{l,k+3} \\
& + 5\psi_{l+1,k} + 25\psi_{l+1,k+1} + 25\psi_{l+1,k+2} + 5\psi_{l+1,k+3} + 5\psi_{l+2,k} + 25\psi_{l+2,k+1} \\
& + 25\psi_{l+2,k+2} + 5\psi_{l+2,k+3} + \psi_{l+3,k} + 5\psi_{l+3,k+1} + 5\psi_{l+3,k+2} + \psi_{l+3,k+3})^2 \Big],
\end{aligned}
$$

$$
\begin{aligned}
z_{3l,4k} = \frac{q}{16} \Big[& (\rho_{l,k+1} + 5\rho_{l,k+2} + 5\rho_{l,k+3} + \rho_{l,k+4} + 5\rho_{l+1,k+1} + 25\rho_{l+1,k+2} + 25\rho_{l+1,k+3} \\
& + 5\rho_{l+1,k+4} + 5\rho_{l+2,k+1} + 25\rho_{l+2,k+2} + 25\rho_{l+2,k+3} + 5\rho_{l+2,k+4} + \rho_{l+3,k+1} \\
& + 5\rho_{l+3,k+2} + 5\rho_{l+3,k+3} + \rho_{l+3,k+4})^2 + (\psi_{l,k+1} + 5\psi_{l,k+2} + 5\psi_{l,k+3} + \psi_{l,k+4} \\
& + 5\psi_{l+1,k+1} + 25\psi_{l+1,k+2} + 25\psi_{l+1,k+3} + 5\psi_{l+1,k+4} + 5\psi_{l+2,k+1} + 25\psi_{l+2,k+2} \\
& + 25\psi_{l+2,k+3} + 5\psi_{l+2,k+4} + \psi_{l+3,k+1} + 5\psi_{l+3,k+2} + 5\psi_{l+3,k+3} + \psi_{l+3,k+4})^2 \Big],
\end{aligned}
$$

$$
\begin{aligned}
z_{4l,1k} = \frac{q}{16} \Big[& (\rho_{l+1,k-2} + 5\rho_{l+1,k-1} + 5\rho_{l+1,k} + \rho_{l+1,w+1} + 5\rho_{l+2,k-2} + 25\rho_{l+2,k-1} + 25\rho_{l+2,k} \\
& + 5\rho_{l+2,k+1} + 5\rho_{l+3,k-2} + 25\rho_{l+3,k-1} + 25\rho_{l+3,k} + 5\rho_{l+3,k+1} + \rho_{l+4,k-2} + 5\rho_{l+4,k-1} \\
& + 5\rho_{l+4,k} + \rho_{l+4,k+1})^2 + (\psi_{l+1,k-2} + 5\psi_{l+1,k-1} + 5\psi_{l+1,k} + \psi_{l+1,k+1} + 5\psi_{l+2,k-2} \\
& + 25\psi_{l+2,k-1} + 25\psi_{l+2,k} + 5\psi_{l+2,k+1} + 5\psi_{l+3,k-2} + 25\psi_{l+3,k-1} + 25\psi_{l+3,k} \\
& + 5\psi_{l+3,k+1} + \psi_{l+4,k-2} + 5\psi_{l+4,k-1} + 5\psi_{l+4,k} + \psi_{l+4,k+1})^2 \Big],
\end{aligned}
$$

$$
\begin{aligned}
z_{4l,2k} = \frac{q}{16} \Big[& (\rho_{l+1,k-1} + 5\rho_{l+1,k} + 5\rho_{l+1,k+1} + \rho_{l+1,k+2} + 5\rho_{l+2,k-1} + 25\rho_{l+2,k} + 25\rho_{l+2,k+1} \\
& + 5\rho_{l+2,k+2} + 5\rho_{l+3,k-1} + 25\rho_{l+3,k} + 25\rho_{l+3,k+1} + 5\rho_{l+3,k+2} + \rho_{l+4,k-1} + 5\rho_{l+4,k} \\
& + 5\rho_{l+4,k+1} + \rho_{l+4,k+2})^2 + (\psi_{l+1,k-1} + 5\psi_{l+1,k} + 5\psi_{l+1,k+1} + \psi_{l+1,k+2} + 5\psi_{l+2,k-1} \\
& + 25\psi_{l+2,k} + 25\psi_{l+2,k+1} + 5\psi_{l+2,k+2} + 5\psi_{l+3,k-1} + 25\psi_{l+3,k} + 25\psi_{l+3,k+1} \\
& + 5\psi_{l+3,k+2} + \psi_{l+4,k-1} + 5\psi_{l+4,k} + 5\psi_{l+4,k+1} + \psi_{l+4,k+2})^2 \Big],
\end{aligned}
$$

$$
\begin{aligned}
z_{4l,3k} = \frac{q}{16} \Big[& (\rho_{l+1,k} + 5\rho_{l+1,k+1} + 5\rho_{l+1,k+2} + \rho_{l+1,k+3} + 5\rho_{l+2,k} + 25\rho_{l+2,k+1} + 25\rho_{l+2,k+2} \\
& + 5\rho_{l+2,k+3} + 5\rho_{l+3,k} + 25\rho_{l+3,k+1} + 25\rho_{l+3,k+2} + 5\rho_{l+3,k+3} + \rho_{l+4,k} + 5\rho_{l+4,k+1}
\end{aligned}
$$

$$+ 5\rho_{l+4,k+2} + \rho_{l+4,k+3})^2 + (\psi_{l+1,k} + 5\psi_{l+1,k+1} + 5\psi_{l+1,k+2} + \psi_{l+1,k+3} + 5\psi_{l+2,k}$$
$$+ 25\psi_{l+2,k+1} + 25\psi_{l+2,k+2} + 5\psi_{l+2,k+3} + 5\psi_{l+3,k} + 25\psi_{l+3,k+1} + 25\psi_{l+3,k+2}$$
$$+ 5\psi_{l+3,k+3} + \psi_{l+4,k} + 5\psi_{l+4,k+1} + 5\psi_{l+4,k+2} + \psi_{l+4,k+3})^2\Big],$$

$$z_{4l,4k} = \frac{q}{16}\Big[(\rho_{l+1,k+1} + 5\rho_{l+1,k+2} + 5\rho_{l+1,k+3} + \rho_{l+1,k+4} + 5\rho_{l+2,k+1} + 25\rho_{l+2,k+2} + 25\rho_{l+2,k+3}$$
$$+ 5\rho_{l+2,k+4} + 5\rho_{l+3,k+1} + 25\rho_{l+3,k+2} + 25\rho_{l+3,k+3} + 5\rho_{l+3,k+4} + \rho_{l+4,k+1} + 5\rho_{l+4,k+2}$$
$$+ 5\rho_{l+4,k+3} + \rho_{l+4,k+4})^2 + (\psi_{l+1,k+1} + 5\psi_{l+1,k+2} + 5\psi_{l+1,k+3} + \psi_{l+1,k+4} + 5\psi_{l+2,k+1}$$
$$+ 25\psi_{l+2,k+2} + 25\psi_{l+2,k+3} + 5\psi_{l+2,k+4} + 5\psi_{l+3,k+1} + 25\psi_{l+3,k+2} + 25\psi_{l+3,k+3}$$
$$+ 5\psi_{l+3,k+4} + \psi_{l+4,k+1} + 5\psi_{l+4,k+2} + 5\psi_{l+4,k+3} + \psi_{l+4,k+4})^2\Big].$$

The semi-discrete system (2.21) is advanced in time using the CN method. Specifically, the midpoint approximations and finite-difference formulas are given by

$$\begin{aligned} \boldsymbol{\rho} &= \frac{1}{2}\left(\boldsymbol{\rho}^{n+1} + \boldsymbol{\rho}^n\right), \qquad \boldsymbol{\psi} = \frac{1}{2}\left(\boldsymbol{\psi}^{n+1} + \boldsymbol{\psi}^n\right), \\ \dot{\boldsymbol{\rho}} &= \frac{\boldsymbol{\rho}^{n+1} - \boldsymbol{\rho}^n}{\Delta t}, \qquad \dot{\boldsymbol{\psi}} = \frac{\boldsymbol{\psi}^{n+1} - \boldsymbol{\psi}^n}{\Delta t}. \end{aligned} \tag{2.26}$$

Substituting (2.26) into the semi-discrete system (2.21), the following fully discrete scheme is obtained:

$$\begin{aligned} 2A\,\boldsymbol{\psi}^{n+1} + \Delta t(B - D(\mathbf{z}))\boldsymbol{\rho}^{n+1} &= 2A\,\boldsymbol{\psi}^n - \Delta t(B - D(\mathbf{z}))\boldsymbol{\rho}^n, \\ 2A\,\boldsymbol{\rho}^{n+1} - \Delta t(B - D(\mathbf{z}))\boldsymbol{\psi}^{n+1} &= 2A\,\boldsymbol{\rho}^n + \Delta t(B - D(\mathbf{z}))\boldsymbol{\psi}^n. \end{aligned} \tag{2.27}$$

The CN scheme is second-order accurate in time and preserves the symmetric structure of the semi-discrete system, making it well-suited for the NLS equation. In the present implementation, the unknown coefficient vectors at the new time level are treated implicitly, whereas the nonlinear coefficient in $D(\mathbf{z})$ is evaluated from the known numerical solution at the previous time level. Therefore, the resulting scheme is linearly implicit rather than fully nonlinear implicit. After enforcing the periodic boundary conditions, the resulting linear system at each time step exhibits a block septa-diagonal structure. The mass matrix A was verified to be symmetric positive definite, while the assembled matrices B and $D(\mathbf{z})$ were symmetric. Together with the condition estimates reported in Table 4, these properties support the nonsingularity of the coefficient matrix; hence, the solution of the linear system exists and admits a unique solution at each time step. The system is solved using a suitable sparse linear solver implemented in MATLAB R2026a.

2.2. *Initial values under periodic boundary conditions*

Initially, the parameter vectors

$$\boldsymbol{\rho}^0 = \left[\rho^0_{0,0}, \rho^0_{0,1}, \ldots, \rho^0_{0,N}, \rho^0_{1,0}, \ldots, \rho^0_{1,N}, \ldots, \rho^0_{N,0}, \ldots, \rho^0_{N,N}\right]^T,$$

$$\boldsymbol{\psi}^0 = \left[\psi^0_{0,0}, \psi^0_{0,1}, \ldots, \psi^0_{0,N}, \psi^0_{1,0}, \ldots, \psi^0_{1,N}, \ldots, \psi^0_{N,0}, \ldots, \psi^0_{N,N}\right]^T$$

are constructed to initialize the system. The initial approximations of the real and imaginary parts are expressed in the bicubic B-spline space as

$$
\begin{aligned}
r_{N,M}(x,y,0) &= \sum_{i=-1}^{N+1}\sum_{j=-1}^{M+1} \rho^0_{i,j}\, B_{i,j}(x,y),\\
s_{N,M}(x,y,0) &= \sum_{i=-1}^{N+1}\sum_{j=-1}^{M+1} \psi^0_{i,j}\, B_{i,j}(x,y),
\end{aligned}
\tag{2.28}
$$

and the coefficients $\boldsymbol{\rho}^0$ and $\boldsymbol{\psi}^0$ are determined by enforcing the interpolation conditions

$$
\begin{aligned}
r_{N,M}(x_l,y_k,0) &= r(x_l,y_k,0),\\
s_{N,M}(x_l,y_k,0) &= s(x_l,y_k,0),
\end{aligned}
\tag{2.29}
$$

for $l = 0, 1, \ldots, N$ and $k = 0, 1, \ldots, M$.

After enforcing the conditions at the grid points (x_l, y_k), the resulting linear systems possess a block tridiagonal structure with cyclic coupling between the first and last blocks. This structure directly reflects the compact support of the bicubic B-spline basis and the imposed periodicity in both the x and y directions as follows.

$$
\begin{bmatrix}
N_2 & N_1 & 0 & \cdots & 0 & 0 & N_1\\
N_1 & N_2 & N_1 & \ddots & 0 & 0 & 0\\
0 & N_1 & N_2 & N_1 & \ddots & 0 & 0\\
\vdots & \ddots & \ddots & \ddots & \ddots & \ddots & \vdots\\
0 & 0 & \ddots & N_1 & N_2 & N_1 & 0\\
0 & 0 & 0 & 0 & N_1 & N_2 & N_1\\
N_1 & 0 & 0 & \cdots & 0 & N_1 & N_2
\end{bmatrix}
\begin{bmatrix}
\boldsymbol{\rho}^0_{0,k}\\ \boldsymbol{\rho}^0_{1,k}\\ \boldsymbol{\rho}^0_{2,k}\\ \vdots\\ \boldsymbol{\rho}^0_{l-2,k}\\ \boldsymbol{\rho}^0_{l-1,k}\\ \boldsymbol{\rho}^0_{l,k}
\end{bmatrix}
=
\begin{bmatrix}
\boldsymbol{r}^0_{0,k}\\ \boldsymbol{r}^0_{1,k}\\ \boldsymbol{r}^0_{2,k}\\ \vdots\\ \boldsymbol{r}^0_{l-2,k}\\ \boldsymbol{r}^0_{l-1,k}\\ \boldsymbol{r}^0_{l,k}
\end{bmatrix}
$$

and

$$
\begin{bmatrix}
N_2 & N_1 & 0 & \cdots & 0 & 0 & N_1\\
N_1 & N_2 & N_1 & \ddots & 0 & 0 & 0\\
0 & N_1 & N_2 & N_1 & \ddots & 0 & 0\\
\vdots & \ddots & \ddots & \ddots & \ddots & \ddots & \vdots\\
0 & 0 & \ddots & N_1 & N_2 & N_1 & 0\\
0 & 0 & 0 & 0 & N_1 & N_2 & N_1\\
N_1 & 0 & 0 & \cdots & 0 & N_1 & N_2
\end{bmatrix}
\begin{bmatrix}
\boldsymbol{\psi}^0_{0,k}\\ \boldsymbol{\psi}^0_{1,k}\\ \boldsymbol{\psi}^0_{2,k}\\ \vdots\\ \boldsymbol{\psi}^0_{l-2,k}\\ \boldsymbol{\psi}^0_{l-1,k}\\ \boldsymbol{\psi}^0_{l,k}
\end{bmatrix}
=
\begin{bmatrix}
\boldsymbol{s}^0_{0,k}\\ \boldsymbol{s}^0_{1,k}\\ \boldsymbol{s}^0_{2,k}\\ \vdots\\ \boldsymbol{s}^0_{l-2,k}\\ \boldsymbol{s}^0_{l-1,k}\\ \boldsymbol{s}^0_{l,k}
\end{bmatrix},
$$

where

$$N_1=\begin{bmatrix}4&1&0&\cdots&0&0&1\\1&4&1&\ddots&0&0&0\\0&1&4&1&\ddots&0&0\\\vdots&\ddots&\ddots&\ddots&\ddots&\ddots&\vdots\\0&0&\ddots&1&4&1&0\\0&0&0&0&1&4&1\\1&0&0&\cdots&0&1&4\end{bmatrix},\qquad N_2=\begin{bmatrix}16&4&0&\cdots&0&0&4\\4&16&4&\ddots&0&0&0\\0&4&16&4&\ddots&0&0\\\vdots&\ddots&\ddots&\ddots&\ddots&\ddots&\vdots\\0&0&\ddots&4&16&4&0\\0&0&0&0&4&16&4\\4&0&0&\cdots&0&4&16\end{bmatrix},$$

$$\boldsymbol{\rho}^0_{0,k}=\begin{bmatrix}\rho^0_{0,0}\\\rho^0_{0,1}\\\vdots\\\rho^0_{0,M-1}\\\rho^0_{0,M}\end{bmatrix},\boldsymbol{\rho}^0_{1,k}=\begin{bmatrix}\rho^0_{1,0}\\\rho^0_{1,1}\\\vdots\\\rho^0_{1,M-1}\\\rho^0_{1,M}\end{bmatrix},\boldsymbol{\rho}^0_{l-1,k}=\begin{bmatrix}\rho^0_{N-1,0}\\\rho^0_{N-1,1}\\\vdots\\\rho^0_{N-1,M-1}\\\rho^0_{N-1,M}\end{bmatrix},\boldsymbol{\rho}^0_{l,k}=\begin{bmatrix}\rho^0_{N,0}\\\rho^0_{N,1}\\\vdots\\\rho^0_{N,M-1}\\\rho^0_{N,M}\end{bmatrix},$$

$$\boldsymbol{s}^0_{0,k}=\begin{bmatrix}s^0_{0,0}\\s^0_{0,1}\\\vdots\\s^0_{0,M-1}\\s^0_{0,M}\end{bmatrix},\boldsymbol{s}^0_{1,k}=\begin{bmatrix}s^0_{1,0}\\s^0_{1,1}\\\vdots\\s^0_{1,M-1}\\s^0_{1,M}\end{bmatrix},\boldsymbol{s}^0_{l-1,k}=\begin{bmatrix}s^0_{N-1,0}\\s^0_{N-1,1}\\\vdots\\s^0_{N-1,M-1}\\s^0_{N-1,M}\end{bmatrix},\boldsymbol{s}^0_{l,k}=\begin{bmatrix}s^0_{N,0}\\s^0_{N,1}\\\vdots\\s^0_{N,M-1}\\s^0_{N,M}\end{bmatrix},$$

$$\boldsymbol{\psi}^0_{0,k}=\begin{bmatrix}\psi^0_{0,0}\\\psi^0_{0,1}\\\vdots\\\psi^0_{0,M-1}\\\psi^0_{0,M}\end{bmatrix},\boldsymbol{\psi}^0_{1,k}=\begin{bmatrix}\psi^0_{1,0}\\\psi^0_{1,1}\\\vdots\\\psi^0_{1,M-1}\\\psi^0_{1,M}\end{bmatrix},\boldsymbol{\psi}^0_{l-1,k}=\begin{bmatrix}\psi^0_{N-1,0}\\\psi^0_{N-1,1}\\\vdots\\\psi^0_{N-1,M-1}\\\psi^0_{N-1,M}\end{bmatrix},\boldsymbol{\psi}^0_{l,k}=\begin{bmatrix}\psi^0_{N,0}\\\psi^0_{N,1}\\\vdots\\\psi^0_{N,M-1}\\\psi^0_{N,M}\end{bmatrix},$$

$$\boldsymbol{r}^0_{0,k}=\begin{bmatrix}r^0_{0,0}\\r^0_{0,1}\\\vdots\\r^0_{0,M-1}\\r^0_{0,M}\end{bmatrix},\boldsymbol{r}^0_{1,k}=\begin{bmatrix}r^0_{1,0}\\r^0_{1,1}\\\vdots\\r^0_{1,M-1}\\r^0_{1,M}\end{bmatrix},\boldsymbol{r}^0_{l-1,k}=\begin{bmatrix}r^0_{N-1,0}\\r^0_{N-1,1}\\\vdots\\r^0_{N-1,M-1}\\r^0_{N-1,M}\end{bmatrix},\quad\text{and}\quad\boldsymbol{r}^0_{l,k}=\begin{bmatrix}r^0_{N,0}\\r^0_{N,1}\\\vdots\\r^0_{N,M-1}\\r^0_{N,M}\end{bmatrix}.$$

The system described above can be solved in MATLAB. The approximate solutions for $r_{N,M}(x_l, y_k, t)$ and $s_{N,M}(x_l, y_k, t)$ are then obtained from the $\rho^{n+1}_{l,k}$ and $\psi^{n+1}_{l,k}$ by solving the system (2.27).

3. Stability analysis

The stability properties of the proposed Galerkin CN scheme are examined under periodic boundary conditions in both spatial directions. Under these conditions, the resulting system matrices exhibit block circulant structures, which naturally admit a Fourier-mode representation and allow the application of a von-Neumann–type stability analysis [3]. At the same time, the periodic setting preserves the algebraic structure of the discrete operators, enabling the stability behavior to be investigated directly at the matrix level.

Starting from the real-valued form of the NLS system (2.5), we define

$$\mathbf{U} = \begin{bmatrix} s \\ r \end{bmatrix}, \qquad M = \begin{bmatrix} 0 & -1 \\ 1 & 0 \end{bmatrix}.$$

Therefore, system (2.5) takes the following compact form:

$$\mathbf{U}_t + M\Delta\mathbf{U} + F(\mathbf{U})\,\mathbf{U} = 0, \tag{3.1}$$

where

$$F(\mathbf{U}) = \begin{bmatrix} 0 & -q(r^2+s^2) \\ q(r^2+s^2) & 0 \end{bmatrix} = \begin{bmatrix} 0 & -\zeta_1 \\ \zeta_2 & 0 \end{bmatrix}.$$

To facilitate a linear stability analysis, the nonlinear term is frozen by a standard local linearization $\zeta = \max\{\zeta_1, \zeta_2\}$, whereby the matrix $F(\mathbf{U})$ is approximated by a bounded constant multiple of the skew-symmetric matrix M, namely, $F(\mathbf{U}) \approx \zeta M$. This approximation leads to the linearized system

$$\mathbf{U}_t + M\Delta\mathbf{U} + \zeta M\mathbf{U} = 0. \tag{3.2}$$

Applying the Galerkin finite element discretization based on bicubic B-spline basis functions yields the semi-discrete system

$$A\,\dot{\mathbf{U}} + M(B - \zeta D)\mathbf{U} = 0, \tag{3.3}$$

where A denotes the symmetric positive definite mass matrix, B is the stiffness matrix, and D is a mass-type matrix associated with the linearized nonlinear term. All matrices are assembled under periodic boundary conditions, resulting in block circulant operators that retain the shift-invariance of the continuous problem. Time discretization is then carried out using the CN scheme, which leads to the fully discrete formulation

$$[2A + \Delta t\, M(B - \zeta D)]\mathbf{U}^{n+1} = [2A - \Delta t\, M(B - \zeta D)]\mathbf{U}^n. \tag{3.4}$$

The stability scheme (3.4) is analyzed using the following Fourier-mode approach:

$$\mathbf{U}^n = \mathbf{P}\,G^n \exp\left[\mathrm{i}\left(k_x x + k_y y\right)\right]$$

is admissible, where $\mathbf{P} \in \mathbb{R}^2$ is a constant vector, G denotes the amplification matrix, and k_x and k_y are the Fourier wave numbers in the x and y directions, respectively. Substituting into U^n yields

$$G = (2A + \Delta t\, MD_\kappa)^{-1}(2A - \Delta t\, MD_\kappa), \tag{3.5}$$

where D_κ represents the Fourier symbol associated with the operator $B - \zeta D$. Since the mass matrix A is symmetric positive definite and the matrix M is skew-symmetric, the matrices $2A \pm \Delta t\, MD_\kappa$ have eigenvalues with identical moduli. As a consequence, the amplification matrix G satisfies $\rho(G) = 1$, where $\rho(G)$ denotes the spectral radius. This result shows that the proposed Galerkin CN scheme is unconditionally stable for the linearized problem, independent of the spatial mesh size and the time step.

The stability result obtained above is consistent with the energy-conserving character of the CN method when applied to Hamiltonian-type systems such as the NLS equation. Moreover, the tensor-product structure of the bicubic B-spline basis, together with the imposed periodicity in both spatial directions, ensures that the analysis extends naturally to the fully 2D setting.

4. Numerical results

A plane wave problem is considered to assess the efficiency and accuracy of the method. The accuracy is assessed by means of the error norms L_2 and L_∞, as well as the associated conservation laws, defined, respectively, as follows:

$$L_2 = \left(h_x h_y \sum_{i=1}^{N} \sum_{j=1}^{M} \left| u_{i,j}^{\text{exact}} - u_{i,j}^{\text{num}} \right|^2 \right)^{\frac{1}{2}}$$

and

$$L_\infty = \max_{1 \le i \le N,\ 1 \le j \le M} \left| u_{i,j}^{\text{exact}} - u_{i,j}^{\text{num}} \right|.$$

Moreover, the 2D conserved quantities are expressed as invariants:

$$I_1 = \iint_\Omega |u(x,y,t)|^2 \, dx\, dy$$

and

$$I_2 = \iint_\Omega \left(|u_x|^2 + |u_y|^2 - \frac{q}{2}|u|^4 \right) dx\, dy.$$

Example 4.1 (Plane wave solution)**.** The analytical plane wave solution in 2D to the NLS equation is [29]

$$u(x,y,t) = C \exp[i(k_1 x + k_2 y - \omega t)], \tag{4.1}$$

where C is the constant amplitude of the plane-wave solution, k_1 and k_2 are the wave numbers, and ω is determined by $\omega = k_1^2 + k_2^2 - q|C|^2$.

In the numerical experiments, the parameter values are chosen to be the same as those used by Wang et al. [30]. The 2D NLS equation is considered with the nonlinear coefficient $q = -2$. The computational domain is taken as $[0, 2\pi] \times [0, 2\pi]$, with periodic boundary conditions (2.3) applied in both spatial directions. The plane wave solution is defined by setting the amplitude $C = 1$ and the wave numbers $k_1 = k_2 = 1$. The initial condition is taken as the exact solution evaluated at $t = 0$. Uniform spatial meshes with $h_x = h_y = h$ are used, and the time integration is performed using a constant time step Δt. All computations were carried out in MATLAB R2026a on a 64-bit system equipped with an Intel Core i5-7200U processor (2.50 GHz) and 20 GB of RAM.

Table 1 reports the temporal evolution of the numerical error norms and the discrete invariants for the bicubic B-spline Galerkin method (Bicubic-BSGM) up to the final time $T = 3$, computed with fixed spatial mesh size $h = \pi/30$ and $\Delta t = 10^{-3}$. It is observed that both the L_2 and L_∞ error norms remain uniformly small throughout the simulation interval, indicating that the proposed scheme maintains a high level of accuracy during long-time integration. Moreover, the values of the discrete mass I_1 and I_2 remain constant at the considered time levels. These results indicate that the proposed Bicubic-BSGM preserves the main invariants with high accuracy and yields stable numerical behavior over the considered time interval. Figures 1–3 further illustrate the approximate solution by comparing the real and imaginary parts of the numerical solution with the corresponding exact solutions along the spatial slices $y = \pi$ and $y = \pi/10$ at different time levels with $h = \pi/30$ and $\Delta t = 10^{-3}$. Figure 4 shows the distribution of the absolute error over Ω at $t = 3$, and Figure 5 shows the corresponding error slice along $y = \pi$ obtained using the Bicubic-BSGM method with $h = \pi/30$ and $\Delta t = 0.001$. Good agreement is observed at all times, which is consistent with the small error magnitudes L_2 and L_∞ reported in Table 1. The graphical results show that the numerical solution retains the qualitative structure of the plane wave throughout the simulation. The real and imaginary components preserve their periodic oscillatory profiles and remain in close agreement with the exact solution along the slices $y = \pi$ and $y = \pi/10$. This indicates that the proposed method captures the phase propagation accurately without producing visible spurious oscillations. The smooth and periodic error distribution further suggest that the observed error is mainly associated with a small accumulated phase difference between the exact and approximate solutions as italic increases. This behavior is consistent with the near preservation of the invariants I_1 and I_2, supporting the stable representation of the wave structure.

Table 1. Temporal evolution of numerical errors and invariants of the Bicubic-BSGM with $h = \pi/30$ and $\Delta t = 0.001$.

t	L_∞	L_2	I_1	I_2
0.5	5.469×10^{-3}	3.436×10^{-2}	3.947842×10^{1}	1.181471×10^{2}
1.0	1.094×10^{-2}	6.872×10^{-2}	3.947842×10^{1}	1.181471×10^{2}
1.5	1.641×10^{-2}	1.031×10^{-1}	3.947842×10^{1}	1.181471×10^{2}
2.0	2.187×10^{-2}	1.374×10^{-1}	3.947842×10^{1}	1.181471×10^{2}
2.5	2.734×10^{-2}	1.718×10^{-1}	3.947842×10^{1}	1.181471×10^{2}
3.0	3.281×10^{-2}	2.062×10^{-1}	3.947842×10^{1}	1.181471×10^{2}

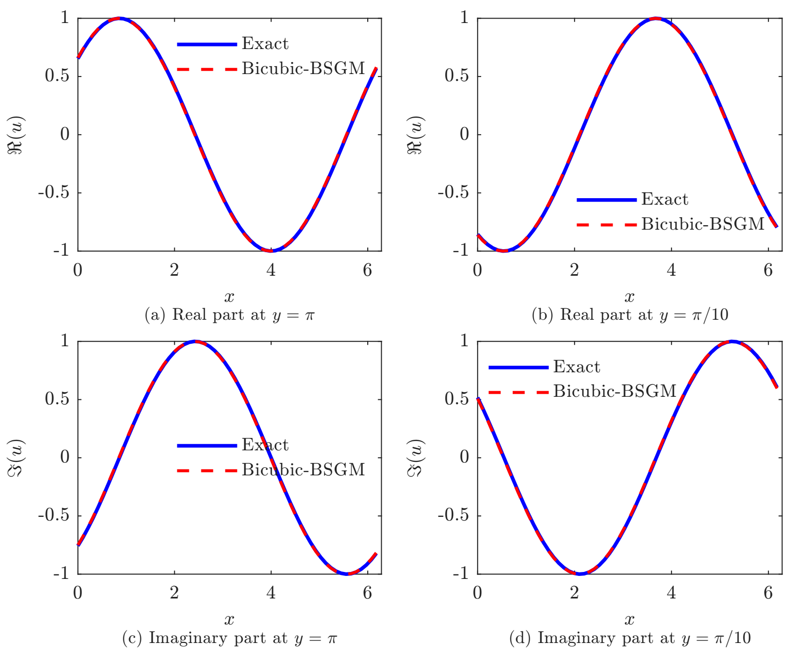

Figure 1. Evolution of the real and imaginary parts of the plane wave solution at $t = 1$ for $y = \pi$ and $y = \pi/10$, computed with $h = \pi/30$ and $\Delta t = 10^{-3}$.

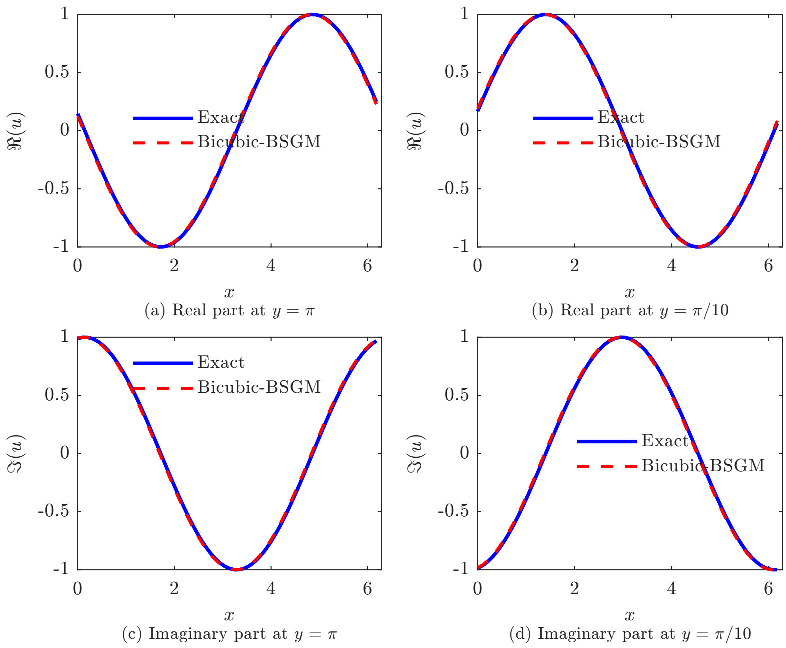

Figure 2. Evolution of the real and imaginary parts of the plane wave solution at $t = 2$ for $y = \pi$ and $y = \pi/10$, computed with $h = \pi/30$ and $\Delta t = 10^{-3}$.

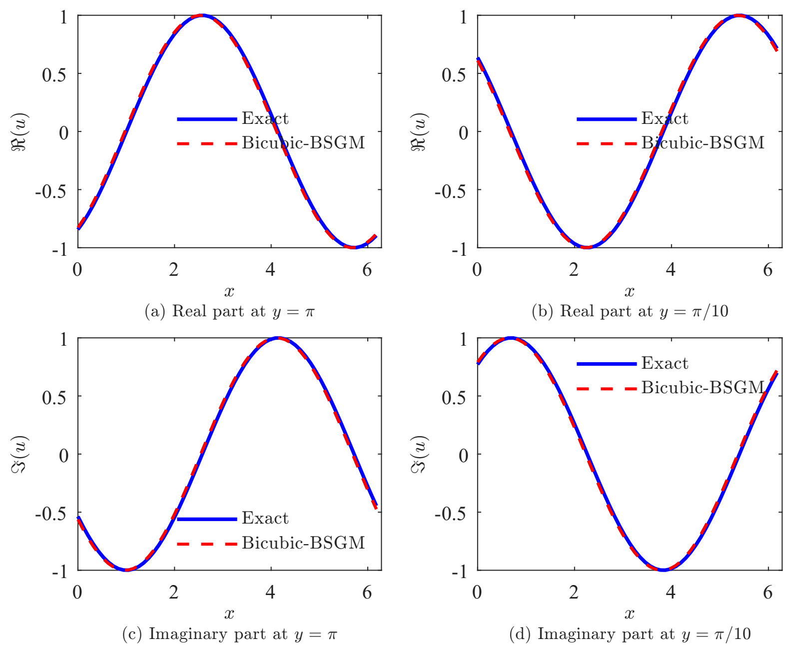

Figure 3. Evolution of the real and imaginary parts of the plane wave solution at $t = 3$ for $y = \pi$ and $y = \pi/10$, computed with $h = \pi/30$ and $\Delta t = 10^{-3}$.

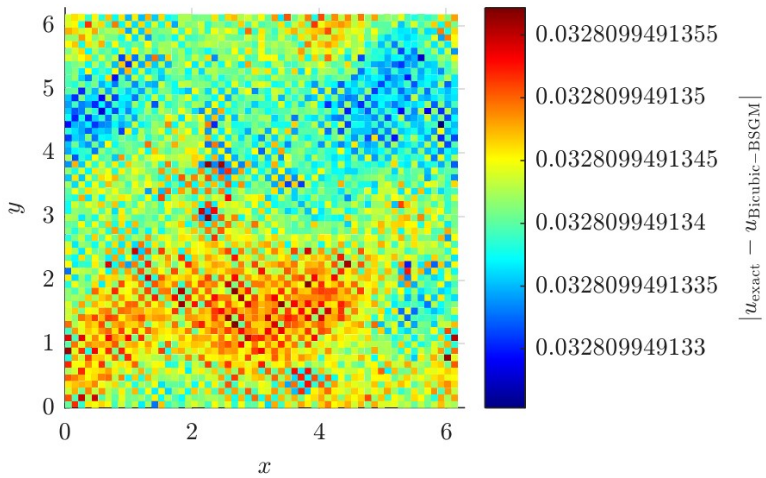

Figure 4. The absolute error over Ω of the Bicubic-BSGM with $h = \pi/30$ and $\Delta t = 0.001$.

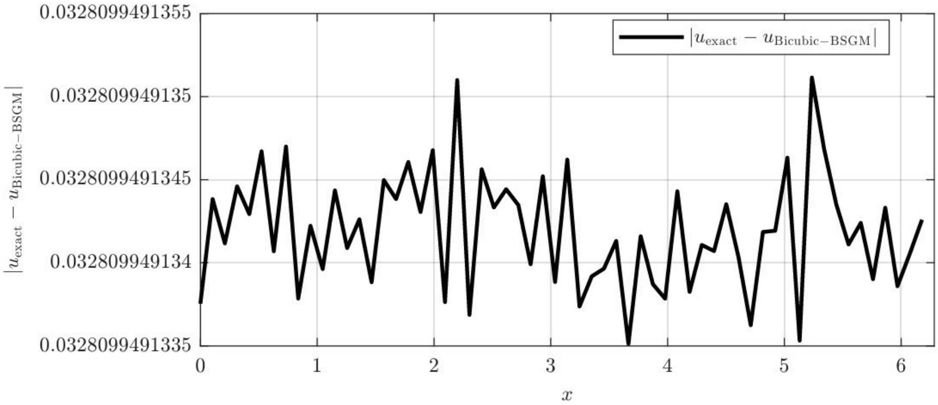

Figure 5. The error slice of the Bicubic-BSGM with $h = \pi/30$ and $\Delta t = 0.001$.

Table 2 presents the numerical errors and the corresponding observed orders of convergence obtained by successively refining the spatial mesh size h, while keeping the time step fixed at $\Delta t = 10^{-5}$. This choice of Δt is sufficiently small to ensure that temporal discretization errors are negligible, so that the reported convergence rates exclusively reflect the spatial accuracy of the proposed scheme.

Table 2. Spatial convergence of the Bicubic-BSGM at $t = 1$ with $\Delta t = 10^{-5}$.

h	L_∞	Order	L_2	Order
1.5708	1.3614×10^{0}	–	8.5538×10^{0}	–
0.7854	5.3622×10^{-1}	1.34	3.3692×10^{0}	1.34
0.3927	1.4920×10^{-1}	1.85	9.3742×10^{-1}	1.85
0.1963	3.8233×10^{-2}	1.96	2.4023×10^{-1}	1.96
0.09817	9.6096×10^{-3}	1.99	6.0379×10^{-2}	1.99

As the mesh is refined, the observed convergence orders in both the L_2 and L_∞ norms approach the theoretical value of two, demonstrating second-order spatial convergence. The slightly reduced convergence rates observed on coarse meshes are attributed to pre-asymptotic effects, whereas the optimal spatial convergence order is fully recovered on sufficiently fine grids.

Table 3 lists the temporal convergence results at $t = 1$ obtained with a fixed spatial step size $h = \pi/120$. To assess the temporal order on a sufficiently fine spatial mesh, the computations were carried out on the reduced spatial domain $[0, \pi]$. This reduction was adopted because of the size of the resulting discrete system on the full domain, which prevents computations with spatial step sizes finer than $h = \pi/60$. Reducing the spatial domain makes it possible to use finer spatial discretizations, so that the observed convergence behavior is mainly governed by the temporal discretization error. The results in the table show that the observed orders in both the L_2 and L_∞ norms are close to two, indicating second-order temporal accuracy. In terms of temporal convergence, the present method exhibits rates close to second order, in agreement with the second-order temporal accuracy reported by [30]. The main distinction between the two approaches lies in the spatial representation: Wang et al. [30] used a compact finite difference framework on discrete grid points, whereas the present method provides a continuous spline-based approximation over the computational domain.

Table 3. Temporal convergence results of the Bicubic-BSGM method at $t = 1$ with $h = \pi/120$.

Δt	L_∞	Order	L_2	Order
0.200	1.757928×10^{0}	–	5.522692×10^{0}	–
0.100	7.131606×10^{-1}	1.30	2.240460×10^{0}	1.30
0.050	2.030467×10^{-1}	1.81	6.378900×10^{-1}	1.81
0.025	5.425479×10^{-2}	1.91	1.704464×10^{-1}	1.91
0.020	3.580866×10^{-2}	1.86	1.124962×10^{-1}	1.86

The conditioning of the Crank–Nicolson linear system is examined by estimating the 1-norm condition number of the block coefficient matrix in Eq (2.29),

$$\mathcal{M}^n = \begin{bmatrix} 2A & -\Delta t(B - D(\mathbf{z}^n)) \\ \Delta t(B - D(\mathbf{z}^n)) & 2A \end{bmatrix}.$$

Since the matrices are large and sparse, the MATLAB function `condest` is used to obtain a 1-norm condition estimate instead of computing the exact condition number. In the implementation, the nonlinear matrix $D(\mathbf{z}^n)$ is assembled from the numerical solution at the previous time level and is kept fixed during the solution of the linear system at the current time step.

As reported in Table 4, the estimated condition numbers remain moderate and of the same order for the tested mesh sizes. This indicates that the Crank–Nicolson systems do not exhibit severe ill-conditioning as the mesh is refined from $h = \pi/10$ to $h = \pi/30$. For the plane-wave test, the estimates are the same at $t = 0$ and $t = 3$ because the modulus of the solution is constant; hence, the element-wise nonlinear coefficient and the corresponding coefficient matrix do not change in time.

Table 4. Estimated 1-norm condition numbers of the CN block coefficient matrix for different mesh sizes with $\Delta t = 10^{-3}$.

h	Matrix size	$t = 0$	$t = 3$
$\pi/10$	800×800	3.782550×10^2	3.782550×10^2
$\pi/20$	3200×3200	4.318313×10^2	4.318313×10^2
$\pi/30$	7200×7200	3.939830×10^2	3.939830×10^2

Example 4.2 (Spatially varying amplitude)**.** To further assess the performance of the proposed method beyond the constant-modulus plane-wave solution, we consider a benchmark problem with spatially varying amplitude, following [29–31]. The initial condition is given by

$$u(x, y, 0) = (1 + \sin x)(2 + \sin y), \qquad (x, y) \in [0, 2\pi] \times [0, 2\pi], \tag{4.2}$$

with periodic boundary conditions and $q = -1$. Unlike the plane-wave solution, the modulus of this initial condition is not constant. Therefore, the nonlinear term $q|u|^2u$ does not reduce to a constant phase contribution, and the test provides a more demanding assessment of the nonlinear two-dimensional dynamics. For this problem, the initial mass and Hamiltonian are given by $I_1(0) = 27\pi^2$ and $I_2(0) = \left(12 + \frac{7945}{32}\right)\pi^2$. The computation is carried out using $h = \pi/60$ and $\Delta t = 5 \times 10^{-4}$ up to the final time $T = 7$. For the nonconstant-amplitude benchmark, the spatial and temporal step sizes were refined systematically to improve the accuracy of the computation and to obtain reliable long-time results for the discrete invariants. Such refinement is particularly necessary for the present nontrivial test, since the spatially varying amplitude introduces stronger nonlinear and gradient effects than the constant-amplitude plane-wave solution. Consequently, nontrivial two-dimensional NLS simulations generally require smaller spatial and temporal step sizes than the simpler plane-wave case. Since no closed-form exact solution is available for this benchmark at later times, the numerical assessment focuses on the peak amplitude and the long-time behavior of the discrete mass and Hamiltonian invariants. The relative invariant errors are computed with respect to the numerical initial values as $E^{\mathrm{rel}}_{I_i}(t) = |I_i(t) - I_i(0)|/|I_i(0)|$, $i = 1, 2$.

Table 5 presents the long-time behavior of the numerical invariants for the spatially varying amplitude benchmark. The mass invariant I_1 remains highly stable throughout the simulation; at $t = 7$, its relative error is still below 10^{-5}. By contrast, the Hamiltonian invariant I_2 shows a gradual increase in error as time advances. This difference reflects the greater sensitivity of I_2, which involves both spatial derivative terms and the nonlinear potential contribution. Such a distinction between mass and energy preservation is commonly reported in numerical studies of NLS-type equations, where energy-conserving schemes usually rely on specifically constructed conservative discretizations and/or nonlinear treatments [30, 32, 33]. Therefore, this benchmark provides a more demanding test of the proposed bicubic B-spline Galerkin method than the constant-modulus plane-wave solution.

Figure 6 highlights the distinct long-time behavior of the discrete mass and Hamiltonian invariants. The relative error associated with the mass invariant remains at a low level throughout the simulation, whereas the Hamiltonian invariant exhibits a progressive increase in error as time advances.

Table 5. Long-time behavior of the peak amplitude and numerical invariants for the spatially varying amplitude benchmark using the Bicubic-BSGM with $h = \pi/60$ and $\Delta t = 5 \times 10^{-4}$.

t	$\max \lvert u \rvert$	I_1^{num}	$E_{I_1}^{rel}$	I_2^{num}	$E_{I_2}^{rel}$
0	6.0000000000	2.6647931883×10^2	0.0000×10^0	2.5688729606×10^3	0.0000×10^0
1	4.3513150993	2.6647963853×10^2	1.1997×10^{-6}	2.6003232178×10^3	1.2243×10^{-2}
2	4.3436177002	2.6647981100×10^2	1.8469×10^{-6}	2.6491311283×10^3	3.1243×10^{-2}
3	4.9501440609	2.6647988017×10^2	2.1065×10^{-6}	2.7235412307×10^3	6.0209×10^{-2}
4	4.6239125043	2.6648021904×10^2	3.3782×10^{-6}	2.8385928501×10^3	1.0500×10^{-1}
5	4.3588156193	2.6648053049×10^2	4.5469×10^{-6}	3.0068116539×10^3	1.7048×10^{-1}
6	5.0187869364	2.6648095807×10^2	6.1515×10^{-6}	3.2386435657×10^3	2.6073×10^{-1}
7	5.2584657690	2.6648189200×10^2	9.6562×10^{-6}	3.5841064865×10^3	3.9521×10^{-1}

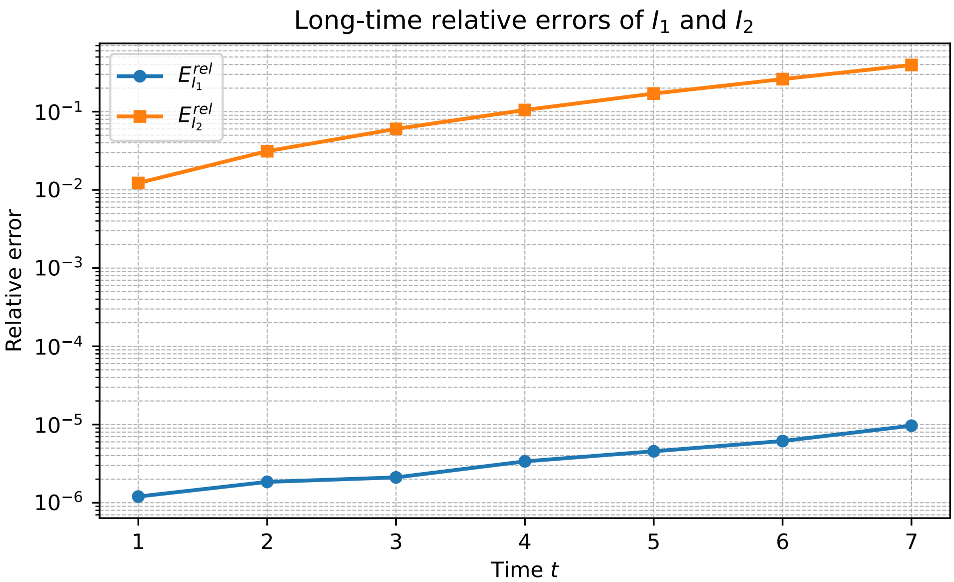

Figure 6. Long-time behavior of the relative errors in the discrete mass and Hamiltonian invariants for the spatially varying amplitude benchmark using the Bicubic-BSGM with $h = \pi/60$ and $\Delta t = 5 \times 10^{-4}$.

5. Conclusions

The numerical experiments indicate that the proposed Bicubic-BSGM achieves high numerical accuracy and remains stable over the specified time interval when sufficiently fine spatial meshes are employed. The condition estimates for the Crank-Nicolson block systems remained moderate for the tested mesh sizes, indicating that mesh refinement did not lead to severe ill-conditioning of the resulting linear systems. In particular, the numerical solution improves systematically as the spatial step size is reduced, suggesting that the spatial discretization error plays a dominant role once the time step is chosen sufficiently small. When compared with the compact finite difference method of

Wang et al. [30], the proposed method offers the additional advantage of representing the numerical solution by smooth bicubic B-spline basis functions rather than only by values at discrete grid points. Overall, the proposed bicubic B-spline Galerkin FEM provides a reliable numerical framework for the simulation of the 2D NLS equation. The spatially varying amplitude benchmark further extends the numerical assessment beyond the constant-modulus plane-wave solution. The observed sensitivity of the Hamiltonian invariant suggests that higher-degree B-spline bases may be examined in future work to enhance the long-time behavior of energy-related quantities for nonconstant-amplitude solutions.

Author contributions

Emad Altahat: Conceptualization, Formal analysis, Investigation, Methodology, Software, Validation, Writing—original draft. Nur Nadiah Abd Hamid: Methodology, Software, Validation, Writing—review and editing. Adila Aida Azahar and Yazariah Mohd Yatim: Funding acquisition, Methodology, Resources, Supervision, Validation, Writing—review and editing. All authors have read and approved the final version of the manuscript for publication.

Use of Generative-AI tools declaration

No generative artificial intelligence large language models were adopted for manuscript writing, model derivation, simulation and data analysis.

Acknowledgments

The authors would like to thank the Research Creativity and Management Office (RCMO), Universiti Sains Malaysia, for providing financial support for this publication. We also extend our gratitude to the anonymous reviewers for their insightful comments and constructive feedback.

Conflict of interest

The authors declare that there are no conflicts of interest.

References

1. J. Yu, F. Yu, Non-autonomous soliton, wave propagation and collision dynamic for (2+1)-dimensional higher-order nonlinear Schrödinger equation with variable coefficients, *Appl. Math. Lett.*, **174** (2026), 109827. https://doi.org/10.1016/j.aml.2025.109827
2. M. Zhou, F. Yu, Space–time shifted solitons and solution interactions for a generalized nonlocal nonlinear Schrödinger equation, *Appl. Math. Lett.*, **178** (2026), 109937. https://doi.org/10.1016/j.aml.2026.109937
3. J. C. Strikwerda, *Finite difference schemes and partial differential equations*, 2 Eds., SIAM, Philadelphia, 2004.
4. M. Dehghan, A. Taleei, Numerical solution of nonlinear Schrödinger equation by using time-space pseudo-spectral method, *Numer. Methods Partial Differ. Equations*, **26** (2010), 979–992. https://doi.org/10.1002/num.20468

5. V. Thomée, *Galerkin finite element methods for parabolic problems*, Lecture Notes in Mathematics, Vol. 1054, Springer Berlin, Heidelberg, 1984. https://doi.org/10.1007/BFb0071790
6. V. Thomée, *Galerkin finite element methods for parabolic problems*, Springer Series in Computational Mathematics, Vol. 25, Springer Berlin, Heidelberg, 2006. https://doi.org/10.1007/3-540-33122-0
7. A. Zlotnick, I. Zlotnick, Finite element method with discrete transparent boundary conditions for the time-dependent 1D Schrödinger equation, *Kinet. Relat. Mod.*, **5** (2012), 639–667. https://doi.org/10.3934/krm.2012.5.639
8. G. Arora, V. Joshi, R. C. Mittal, Numerical simulation of nonlinear Schrödinger equation in one and two dimensions, *Math. Models Comput. Simul.*, **11** (2019), 634–648. https://doi.org/10.1134/S2070048219040070
9. D. Shi, Z. Qi, Linearized decoupled mass and energy conservation CN Galerkin FEM for the coupled nonlinear Schrödinger system, *J. Sci. Comput.*, **100** (2024), 76. https://doi.org/10.1007/s10915-024-02632-z
10. X. Zhu, Y. Zhang, Y. Nie, Split-step Galerkin FE method for two-dimensional space-fractional CNLS, *Fractal Fract.*, **8** (2024), 402. https://doi.org/10.3390/fractalfract8070402
11. X. Liang, A. Q. M. Khaliq, Q. Sheng, Exponential time differencing Crank–Nicolson method with a quartic spline approximation for nonlinear Schrödinger equations, *Appl. Math. Comput.*, **235** (2014), 235–252. https://doi.org/10.1016/j.amc.2014.02.063
12. E. Lee, D. Kim, Stability analysis of the implicit finite difference schemes for nonlinear Schrödinger equation, *AIMS Math.*, **7** (2022), 16349–16365. https://doi.org/10.3934/math.2022893
13. E. N. Aksan, Quadratic B-spline finite element method for numerical solution of the Burgers' equation, *Appl. Math. Comput.*, **174** (2006), 884–896. https://doi.org/10.1016/j.amc.2005.05.020
14. E. Kırlı, A novel B-spline collocation method for Hyperbolic Telegraph equation, *AIMS Math.*, **8** (2023), 11015–11036. https://doi.org/10.3934/math.2023558
15. B. Lin, Septic spline function method for nonlinear Schrödinger equations, *Appl. Anal.*, **94** (2015), 279–293. https://doi.org/10.1080/00036811.2014.890709
16. A. Bashan, N. M. Yagmurlu, Y. Ucar, A. Esen, An effective approach to numerical soliton solutions for the Schrödinger equation via modified cubic B-spline differential quadrature method, *Chaos Soliton. Fract.*, **100** (2017), 45–56. https://doi.org/10.1016/j.chaos.2017.04.038
17. R. Mohammadi, Smooth quintic spline approximation for nonlinear Schrödinger equations with variable coefficients in one and two dimensions, *Chaos Soliton. Fract.*, **107** (2018), 204–215. https://doi.org/10.1016/j.chaos.2018.01.006
18. A. Iqbal, N. N. Abd Hamid, A. I. M. Ismail, Soliton solution of Schrödinger equation using cubic B-spline Galerkin method, *Fluids*, **4** (2019), 108. https://doi.org/10.3390/fluids4020108
19. N. N. A. Hamid, A. A. Majid, A. I. M. Ismail, Bicubic B-spline interpolation method for two-dimensional Laplace's equations, *AIP Conf. Proc.*, **1522** (2013), 1033–1038. https://doi.org/10.1063/1.4801243
20. R. C. Mittal, A. Tripathi, Numerical solutions of two-dimensional Burgers' equations using modified bi-cubic B-spline finite elements, *Eng. Comput.*, **32** (2015), 1275–1306. https://doi.org/10.1108/EC-04-2014-0067

21. R. C. Mittal, A. Tripathi, Numerical solutions of two-dimensional unsteady convection–diffusion problems using modified bi-cubic B-spline finite elements, *Int. J. Comput. Math.*, **94** (2017), 1–21. https://doi.org/10.1080/00207160.2015.1085976
22. L. R. T. Gardner, G. A. Gardner, A two dimensional bi-cubic B-spline finite element: used in a study of MHD-duct flow, *Comput. Methods Appl. Mech. Eng.*, **124** (1995), 365–375. https://doi.org/10.1016/0045-7825(94)00760-K
23. S. Wang, Split-step quintic B-spline collocation methods for nonlinear Schrödinger equations, *AIMS Math.*, **8** (2023), 19794–19815. https://doi.org/10.3934/math.20231009
24. X. Pan, A high-accuracy conservative numerical scheme for the generalized nonlinear Schrödinger equation with wave operator, *AIMS Math.*, **9** (2024), 27388–27402. https://doi.org/10.3934/math.20241330
25. B. Zhou, S. Pan, Z. Fang, M. Li, Linearized $L1$-Galerkin method for variable order time-fractional Schrödinger equation with unconditional convergence, *AIMS Math.*, **10** (2025), 26527–26544. https://doi.org/10.3934/math.20251166
26. X. Zhao, Numerical integrators for continuous disordered nonlinear Schrödinger equation, *J. Sci. Comput.*, **89** (2021), 40. https://doi.org/10.1007/s10915-021-01653-2
27. Y. He, X. Zhao, Numerical methods for some nonlinear Schrödinger equations in soliton management, *J. Sci. Comput.*, **95** (2023), 61. https://doi.org/10.1007/s10915-023-02181-x
28. J. Dong, Q. Zhang, X. Zhao, Numerical methods for nonlinear Schrödinger equation with shock type initial data, *Comput. Phys. Commun.*, **324** (2026), 110143. https://doi.org/10.1016/j.cpc.2026.110143
29. Y. Xu, C. W. Shu, Local discontinuous Galerkin methods for nonlinear Schrödinger equations, *J. Comput. Phys.*, **205** (2005), 72–97. https://doi.org/10.1016/j.jcp.2004.11.001
30. T. Wang, B. Guo, Q. Xu, Fourth-order compact and energy conservative difference schemes for the nonlinear Schrödinger equation in two dimensions, *J. Comput. Phys.*, **243** (2013), 382–399. https://doi.org/10.1016/j.jcp.2013.03.007
31. R. T. Glassey, On the blowing up of solutions to the Cauchy problem for nonlinear Schrödinger equations, *J. Math. Phys.*, **18** (1977), 1794–1797. https://doi.org/10.1063/1.523491
32. X. Antoine, W. Bao, C. Besse, Computational methods for the dynamics of the nonlinear Schrödinger/Gross–Pitaevskii equations, *Comput. Phys. Commun.*, **184** (2013), 2621–2633. https://doi.org/10.1016/j.cpc.2013.07.012
33. X. Feng, H. Liu, S. Ma, Mass- and energy-conserved numerical schemes for nonlinear Schrödinger equations, *Commun. Comput. Phys.*, **26** (2019), 1365–1396. https://doi.org/10.4208/cicp.2019.js60.05